Unimolecular Reactions of Peroxy Radicals Formed in the Oxidation of #-pinene and #-pinene by Hydroxyl Radicals

Lu Xu, Kristian H. Møller, John D. Crounse, Rasmus V. Otkjær, Henrik Grum Kjaergaard, and Paul O. Wennberg

Just Accepted

1 Unimolecular Reactions of Peroxy Radicals Formed in the Oxidation of α-pinene and β-pinene by

2 Hydroxyl Radicals

3

4 Lu Xu[†,*], Kristian H. Møller[§], John D. Crounse[†], Rasmus V. Otkjær[§], Henrik G. Kjaergaard[§,*],

5 Paul O. Wennberg[†,⊥,*]

6 [†]Division of Geological and Planetary Sciences, California Institute of Technology, Pasadena,

7 California 91125, United States

8 [§]Department of Chemistry, University of Copenhagen, Universitetsparken 5, DK-2100,

9 Copenhagen Ø, Denmark

10 [⊥]Division of Engineering and Applied Science, California Institute of Technology, Pasadena,

11 California 91125, United States

12

1

13 **Abstract**

14 Atmospheric oxidation of monoterpenes (emitted primarily by evergreen trees) is known to

15 contribute to the formation and growth of aerosol particles. While recent research has tied the

16 formation of organic aerosol to unimolecular chemistry of the organic peroxy radicals (RO_2)

17 formed in the oxidation of monoterpenes, the fundamental physical chemistry of these RO_2

18 remains obscure. Here, we use isomer-specific measurements and *ab initio* calculations to

19 determine the unimolecular reaction rates and products of RO_2 derived from the hydroxyl radical

20 (OH) oxidation of α-pinene and β-pinene. Among all the structural isomers of the first-generation

21 RO_2 from both monoterpenes, we find that the first-generation RO_2 produced following opening

22 of the four-membered ring undergo fast unimolecular reactions (4 ± 2 and 16 ± 5 s^{-1} for α-pinene and

23 β-pinene, respectively) at 296 K, in agreement with high level *ab initio* calculations. The presence

24 of the hydroxy group and carbon-carbon double bond in the ring-opened RO_2 enhances the rates

25 of these unimolecular reactions, including endo-cyclization or H-shift via transition states

26 involving six- and seven-membered rings. These reaction rate coefficients are sufficiently fast that

27 unimolecular chemistry is the dominant fate of these monoterpene derived RO_2 in the atmosphere.

28 In addition, the overall yield of first generation α-pinene and β-pinene hydroxy nitrates, $C_{10}H_{17}NO_4$,

29 at 296 K and 745 torr is measured to be $3.3\pm1.5\%$ and $6.4\pm2.1\%$, respectively, for conditions where

30 all RO_2 are expected to react with NO ([NO] > 1000 ppbv). These yields are lower than anticipated.

31

32   **Introduction**

33   Approximately 150 Tg of monoterpenes ($C_{10}H_{16}$) are emitted from biogenic vegetation to Earth's

34   atmosphere every year[1]. Monoterpenes rapidly react with atmospheric oxidants and produce a

35   myriad of oxygenated compounds[2-7] that influence the NO_x cycle[8] and Earth's radiation balance[9].

36   Oxygenated compounds produced from monoterpenes are a major contributor to organic aerosol

37   globally[10-11] and have been suggested to be the largest source of summertime organic aerosol in

38   the southeastern U.S.[7, 12]. Despite extensive investigations, knowledge of the mechanisms and

39   products of monoterpene photooxidation is still incomplete[13]. In particular, the fate of peroxy

40   radicals (RO_2) produced in this chemistry remains speculative. Typically, RO_2 in the atmosphere

41   undergo bimolecular reactions with nitric oxide (NO), hydroperoxy radical (HO_2), and other

42   RO_2[14-15]. Recent studies have shown, however, that RO_2 unimolecular reactions can often compete

43   with these bimolecular reactions[16-20]. Some monoterpene RO_2 have been inferred to undergo fast

44   unimolecular reactions, based on the observed rapid formation of highly oxygenated molecules

45   (HOMs), which carry six or more oxygen atoms in the oxidation of monoterpenes[9, 21-22]. The

46   unimolecular reaction rates of monoterpene RO_2, however, have not been measured.

47   In this study, we experimentally determine the unimolecular reaction rate coefficients of

48   RO_2 derived from the OH oxidation of α-pinene and β-pinene, which together account for more

49   than half of total monoterpene emissions[1]. We perform isomer-specific measurements of a suite of

50   hydroxy nitrates (HNs), produced from RO_2 reaction with NO, to probe the competition between

51   RO_2 bimolecular and unimolecular reactive pathways. We also use *ab initio* multi-conformer

52   transition state theory (MC-TST) [23-24] to aid the understanding of the reaction mechanisms.

Methods

53

54 **Experimental Methods.** We perform a suite of laboratory photooxidation experiments of α-

55 pinene and β-pinene in a 0.8 m^3 collapsible FEP Teflon (Dupont) Environmental Chamber at

56 ambient laboratory pressure (~993 hPa) and temperature (296 K). The VOC ((+) α-pinene (98%,

57 Sigma-Aldrich) or (-) β-pinene (99%, Sigma-Aldrich)) is transferred into the experimental

58 chamber via a gas-tight 500 cm^3 glass bulb. We prepare the bulb by evacuating it to <0.3 torr,

59 evaporating VOC liquid into the bulb, and serial dilution with N_2 to achieve the desired mixing

60 ratio. The concentration of VOC in glass bulb is verified by FTIR spectroscopy using tabulated

61 cross-sections [25]. The initial VOC concentration in the chamber ranges from roughly 60 to 120

62 ppbv.

63   The photolysis of methyl nitrite (CH_3ONO) is used as the primary source of OH. CH_3ONO

64 is synthesized, purified, and stored using methods similar to those described by Taylor et al. [26] The

65 CH_3ONO is injected into the chamber in the same fashion as VOC. The initial CH_3ONO

66 concentration in the chamber is roughly 70 ppbv. For experiments with initial NO, a 500 cm^3 bulb

67 with desired NO concentration is prepared by mixing 1993 ± 20 ppmv NO (Matheson) and N_2 with

68 the desired dilution ratio. The content of the bulb is then transferred to the chamber. The initial

69 NO concentration ranges from 0 to 2.2 ppmv. Dry zero air is added to the evacuated chamber using

70 a mass flow controller (MKS), allowing the initial concentration of species to be calculated to

71 better than 5% uncertainty. The detailed concentrations of VOC, NO, and CH_3ONO in all

72 experiments are shown in Table S1. After all of the reagents are injected and well-mixed in the

73 chamber, UV lights (Sylvania F40/350BL) are turned on to initiate photooxidation. To study the

74 RO_2 unimolecular reactions under low concentrations of NO and HO_2, we use only one UV bulb.

75 The OH concentration ranges from 1×10^6 to 8×10^6 molecule cm^{-3}, due to different NO levels

4

76 between experiments. To achieve similar OH exposure (i.e., 2×10^9 and 1×10^9 molecules cm^{-3} s for

77 α-pinene and β-pinene experiments, respectively), we vary the oxidation time between 2.5 min to

78 30 min. Under these OH exposure levels, roughly 10% of initial VOC is oxidized.

79 **Instrumentation.** The analytical instruments, including an O$_3$ monitor (Teledyne O$_3$ M400E), a

80 chemilumnescence NO/NO$_x$ monitor (Teledyne NO$_x$ M200EU), a Gas Chromatograph with a

81 Flame Ionization Detector (GC-FID, Hewlett Packard 5890 series II Plus), and a Gas-

82 Chromatography Time of Flight Chemical Ionization Mass Spectrometer (GC-ToF-CIMS), are

83 connected to experimental chamber using ~2 m of 1/4 inch PFA tubing. We use the GC-FID to

84 measure α-pinene and β-pinene. Because CH$_3$ONO can cause interference in the measured

85 concentrations of NO and NO$_2$, the NO$_x$ monitor is only used to measure the initial NO and NO$_2$

86 concentration (before CH$_3$ONO injection). The O$_3$ concentration measured by the O$_3$ monitor is

87 close to zero in all experiments, which limits VOC consumption by O$_3$ to less than 1% during these

88 experiments.

89 We use GC-ToF-CIMS with CF$_3$O$^-$ as the reagent ion, which is sensitive to multifunctional

90 oxygenated products. CF$_3$O$^-$ is produced by flowing 1 ppmv CF$_3$OOCF$_3$ (in N$_2$) through a

91 radioactive ^{210}Po source. Then, CF$_3$O$^-$ selectively interacts with analytes at a pressure of 35 mbar

92 to generally form either cluster ions (R1) or fluoride transfer ions (R2).

93
$$VOC + CF_3O^- \leftrightarrow VOC \cdot CF_3O^- \qquad (R1)$$
$$VOC + CF_3O^- \rightarrow VOC_{-H}^- \cdot HF + CF_2O \quad (R2)$$

94 The GC-ToF-CIMS has two sampling modes, direct sampling and GC sampling. In direct

95 sampling mode, CIMS samples air directly from the reaction chamber recording spectra at 10 Hz

96 temporal resolution. In GC sampling mode, the CIMS samples the effluent of a GC. In brief, the

97 analytes are pulled from the reaction chamber and cryo-trapped on the head of a 1 m Restek RTX-

98   1701 column at -20°C. After trapping for certain time (typically 10 min, 2 L chamber air), elution

99   is enabled using a flow of 5 sccm N_2 and a temperature ramping program (SI section S1). The GC

100   effluent is diluted with additional N_2 and transferred into the CIMS. More details about the

101   operation and principles of CF_3O^- GC-ToF-CIMS can be found in Vasquez et al[27]. In both sampling

102   modes, the observed ion signals are normalized to the sum of isotopes of the reagent ion (i.e.,

103    $^{13}CF_3O^-$ and $^{13}CF_3O^- \cdot H_2O$), to account for variation in the total ion signal. The high mass resolution

104   data analysis is performed using the Tofware software (Tofwerk).

105   **Peroxy radical bimolecular lifetime.** We perform a series of experiments under different RO_2

106   bimolecular lifetimes ($\tau_{bimolecular}$, Eqn.(1)) by varying [NO] and [HO_2].

107
$$\tau_{bimolecular} = \frac{1}{k_{RO_2+NO}[NO] + k_{RO_2+HO_2}[HO_2]} \quad \text{Eqn. (1)}$$

108   The [NO] and [HO_2] during photooxidation are simulated using Master Chemical Mechanism

109   (MCM, version 3.2)[28-29] updated with nitrate branching ratios and ring-opening fractions of

110   activated terpene alkyl radicals based on results from this study. k_{RO2+NO} and $k_{RO2+HO2}$ are taken

111   from the MCM[29] as 9.15×10^{-12} and 2.39×10^{-11} cm^3 $molec^{-1}$ s^{-1} at 296 K, respectively. We assume

112   k_{RO2+NO} and $k_{RO2+HO2}$ to be isomer independent. RO_2+RO_2 chemistry is calculated to be of

113   negligible importance in these experiments due to small concentrations of RO_2 radicals. We use

114   MCM and estimate that RO_2+RO_2 reactions account for < 2% of RO_2 bimolecular loss, using a

115   rate coefficient of 2×10^{-12} cm^3 $molec^{-1}$ s^{-1}. Details about the MCM updates and $\tau_{bimolecular}$

116   calculation can be found in the SI section S2. For experiments with no initial NO injection (i.e.,

117   Experiments 6 and 13 in Table S1), we estimate [NO] and [HO_2] based on the measured production

118   rates of H_2O_2, hydroxy hydroperoxides, and hydroxy nitrates by following the procedure in

119 Crounse et al.[30] The subsequently calculated $\tau_{bimolecular}$ from this method agree within 25% of the

120 values estimated using MCM (SI section S2).

121 **Computational approach.** Reaction rate coefficients, k, for the RO$_2$ unimolecular reactions are

122 calculated using MC-TST[23-24]:

123 $$k = \kappa \frac{k_B T}{h} \frac{\sum_i^{All\,TS\,conf.} \exp\left(-\frac{\Delta E_i}{k_B T}\right) Q_{TS_i}}{\sum_j^{All\,R\,conf.} \exp\left(-\frac{\Delta E_j}{k_B T}\right) Q_{R_j}} \exp\left(-\frac{E_{TS} - E_R}{k_B T}\right) \quad \text{Eqn. (2)}$$

124 where κ is the tunneling coefficient, k_B is the Boltzmann constant, T is the temperature and h is

125 the Planck constant. The two summations run over all transition states and reactant conformers,

126 respectively, and sum the partition function of a given conformer weighted by its Boltzmann factor

127 calculated relative to the corresponding lowest-energy conformer. The final exponential term has

128 the zero-point corrected energy difference between the lowest-energy TS and reactant conformers,

129 i.e., the reaction barrier.

130 Energies and partition functions in the equation are calculated using the approach described

131 by Møller et al.[23] Briefly, conformers are located by a systematic conformer search using MMFF

132 in Spartan '14 or '16 with a neutral charge enforced [31-38]. The conformer search is followed by

133 optimizations with B3LYP/6-31+G(d) in Gaussian 16, rev. A.03 [39-44]. Slow reactions (i.e. with rate

134 coefficients below 5×10^{-3} s^{-1} at room temperature) are ignored, because the calculated rate

135 coefficients at this level of theory are most often biased high. For the faster reactions, conformers

136 with electronic energies within 2 kcal mol^{-1} of the lowest-energy conformer at the B3LYP/6-

137 31+G(d) level are reoptimized using ωB97X-D/aug-cc-pVTZ [45-47]. In Møller et al., a 2 kcal mol^{-1}

138 cut-off based on electronic energy at this level was found to be suitable [23]. For the conformer

139 lowest in zero-point corrected energy at the ωB97X-D/aug-cc-pVTZ level, an RO-CCSD(T)-

140 F12a/VDZ-F12//ωB97X-D/aug-cc-pVTZ (abbreviated F12) single-point energy calculation is

141 done to get a more accurate barrier height [48-54]. Due to issues with the HF calculations converging

142 to different possible solutions, no F12 single-point energy calculations are conducted for

143 abstraction from OH groups. Consistent with Møller et al.[55], we estimate that the uncertainty on

144 the rate coefficients increases to a factor of 100 without F12 single point energy calculations.

145 The tunneling coefficient is calculated using the Eckart approach based on the conformers

146 connected to the lowest-energy TS using an IRC[56-57]. Eckart barriers are calculated using F12,

147 while the imaginary frequency of the TS is calculated at the ωB97X-D/aug-cc-pVTZ level. The

148 conformer searches are performed using Spartan '14 or '16, the DFT calculations are done with

149 Gaussian 16, rev. A.03 and the F12 calculations are conducted using Molpro 2012. For reaction

150 A1, the DFT calculations are performed using Gaussian 09, rev. D.01.

151 The competition between ring-opening and addition of O_2 for the hydroxy alkyl radicals

152 formed by addition of OH to α-pinene and β-pinene is modeled using RRKM theory within the

153 MESMER software package[58] with electronic structure theory as described in the approach of

154 Møller et al.[23] A full description of the theoretical approach is included in SI section S3. The dipole

155 moment and polarizability of oxidation products, for use in estimating instrumental sensitivity, are

156 calculated using B3LYP/cc-pVTZ (SI section S3).

157 Following the recommendations of previous studies and comparisons with experiments,

158 we estimate the uncertainty on rate coefficients of this approach to be a factor of 10 [18, 23, 59]. Our

159 calculated results are broadly consistent with previous studies by Vereecken et al.[5, 60], Peeters et

160 al.[61], and Berndt et al.[21], but use higher level of theory and include important pathways not

161 previously considered.

162

8

Results and Discussion

The isomer distribution of $C_{10}H_{17}NO_4$ hydroxy nitrates. The oxidation of both monoterpenes

initiated by OH addition produces a set of RO_2 isomers and, following reaction with NO, hydroxy

nitrates (HNs). Here, we only describe the formation of $C_{10}H_{17}NO_4$. As discussed later, additional

nitrates are formed following isomerization chemistry of peroxy and alkoxy radicals. A simplified

oxidation mechanism for α-pinene + OH is shown in Scheme 1. The OH addition onto the double

bond produces four hydroxy alkyl radicals, two diastereomer pairs of 2-OH,3-R• and 3-OH,2-R•.

It is expected that 2-OH,3-R• mainly undergoes collisional stabilization, followed by O_2 addition

to produce 2-OH,3-RO_2. 3-OH,2-R•, however, can undergo either collisional stabilization and O_2

addition to produce 3-OH,2-RO_2 or, via C-C scission (ring opening) and O_2 addition, form 3-OH,8-

RO_2[4]. In total, three distinct structural isomers of RO_2 (each comprised of several stereoisomers)

are produced. As a result, three structural isomers of HNs are formed via RO_2 reaction with NO.

A similar scheme for β-pinene is shown in Scheme S1.

The HNs are separated using gas chromatography and quantified by GC-ToF-CIMS

(Figure 1). Three distinct peaks are observed to be produced from the OH oxidation of both

monoterpenes in the presence of NO. The structural assignment of the HN isomers is achieved

through several experiments. The ring-opened HN is unsaturated and thus reacts with O_3 while the

ring-retained HN isomers are saturated and will not do so (Figure S1). Thus, the third peak is

assigned to ring-opened HN (i.e., 3-OH,8-ONO_2 for α-pinene) because it disappears upon adding

O_3 to the chamber following photooxidation. The first peak in the chromatogram is assigned to the

HN with the $-ONO_2$ group on the less-substituted carbon (i.e., 2-OH,3-ONO_2 for α-pinene). This

assignment is based on the elution time of the major HN produced from NO_3-initiated oxidation

experiments (Figure S2), where the first peak corresponds to the dominant peak produced from

186 NO$_3$ chemistry, consistent with the assumption that NO$_3$ reacts with alkenes by primarily adding

187 to the less-substituted olefinic carbon[62]. Finally, the second peak is assigned to the HN with the –

188 OH group on the less-substituted carbon (i.e., 3-OH,2-ONO$_2$ for α-pinene). This assignment is

189 based on the previous finding that the retention order for HNs with similar structures generally

190 follows the order: tertiary –OH, secondary –OH, and then primary –OH for the same GC column[63]

191 (Figure S3). This observation has a plausible rationale as the secondary –OH has stronger

192 interaction with GC column than tertiary OH due to less shielding effects. More details on

193 chromatographic assignment are provided in the SI section S1. In summary, for each monoterpene,

194 the first two peaks are the two structural isomers of ring-retained β-HNs (e.g., 2-OH,3-ONO$_2$ and

195 3-OH,2-ONO$_2$ for α-pinene), each likely comprised of multiple diastereomers; the third peak is

196 the ring-opened HN (e.g., 3-OH,8-ONO$_2$ for α-pinene), likely containing 2 diastereomers for the

197 α-pinene system.

198 For conditions where all RO$_2$ are expected to react with NO ([NO] > 1000 ppbv), the GC

199 transmission efficiencies of α-pinene and β-pinene hydroxy nitrates (C$_{10}$H$_{17}$NO$_4$) are 79±4% and

200 99±5%, respectively (SI section S1).

201 **Rate Coefficients of Unimolecular Reactions.** We find that the yields of ring-retained β-HNs

202 (i.e., the amount of HNs produced divided by the amount of monoterpene oxidized) do not change

203 with RO$_2$ bimolecular lifetime ($\tau_{bimolecular}$), after accounting for the fraction of RO$_2$ that reacts with

204 NO (Figure S4). This finding suggests that the unimolecular reaction rates of ring-retained RO$_2$

205 are much slower than bimolecular chemistry for conditions investigated here ($\tau_{bimolecular}$: 0.001 –

206 10 s). This experimental result is corroborated by our MC-TST calculations using ωB97X-D/aug-

207 cc-pVTZ; the unimolecular reaction rate coefficients for ring-retained RO$_2$ in both monoterpenes

208 are calculated to be slower than 0.05 s^{-1} with the exception of one isomer of α-pinene which has a

209 calculated H-shift rate coefficient of 0.12 s^{-1} (Table S8 and S9). In contrast, we find that the yield

210 of ring-opened HN (i.e., α-pinene 3-OH,8-ONO$_2$ and β-pinene 1-OH,8-ONO$_2$) decreases with

211 $\tau_{bimolecular}$. Figure 1(a) and (b) present the HN distributions under three different $\tau_{bimolecular}$ for the

212 α-pinene and β-pinene systems, respectively. The yield of ring-opened HNs decreases with longer

213 $\tau_{bimolecular}$, because the unimolecular reactions shorten the time available for the ring-opened RO$_2$

214 to react with NO. This observation is corroborated by our theoretical calculation as will be shown

215 later.

216   To determine the unimolecular reaction rates of ring-opened RO$_2$, we utilize the ratio of

217 the ring-opened HN signal relative to that of the ring-retained HNs. Ring-retained HNs are used

218 as a reference for the RO$_2$ + NO bimolecular reaction, as the unimolecular reactions of ring-

219 retained RO$_2$ are negligible for the conditions investigated here. In contrast, the formation of ring-

220 opened HN depends on the competition between reaction with NO and unimolecular chemistry.

221 Thus, the change in the (ring-opened HN):(ring-retained HNs) ratio as a function of $\tau_{bimolecular}$ is a

222 measure of the ratio of the unimolecular reactions of ring-opened RO$_2$ to its bimolecular reaction

223 with NO. Detailed mathematical derivations are shown in the SI section S2. The (ring-opened

224 HN):(ring-retained HNs) ratio decreases as $\tau_{bimolecular}$ increases due to increased importance of the

225 unimolecular reactions of the ring-opened RO$_2$ at longer $\tau_{bimolecular}$ (Figure 2). When $\tau_{bimolecular}$ is

226 ~10 s, the formation of ring-opened HN is suppressed because all ring-opened RO$_2$ undergoes

227 unimolecular reactions. We use a kinetic model to simulate the relationship between (ring-opened

228 HN):(ring-retained HNs) and $\tau_{bimolecular}$ (SI section S4) with varying unimolecular reaction rates.

229 The unimolecular reaction rate coefficient is the only fitted parameter in the model. By comparing

230 the simulated and measured relationships, we determine the rates of unimolecular reactions to be

231 4±2 s^{-1} and 16±5 s^{-1} at 296 K for α-pinene and β-pinene ring-opened RO$_2$, respectively (Figure 2).

11

232　An equivalent NO reactivity at 296 K requires mixing ratios of 18 and 70 ppbv NO, respectively

233　– values substantially larger than found over forested regions where monoterpenes are emitted and

234　even over many polluted urban areas [64-65].

235　　　These rates are consistent with the previously estimated ranges from theoretical

236　calculations (1-10 s^{-1} for α-pinene ring-opened RO$_2$ in Berndt et al.[21] and Vereecken et al.[60]) and

237　from simulating α-pinene ozonolysis with a few fitting parameters (3-10 s^{-1} in Zhao et al.[22]). The

238　measured rates agree well with our theoretical calculations using higher level of theory as

239　presented in the next section.

240　**Unimolecular reaction channels.** For the ring-opened RO$_2$ from both monoterpenes, there are a

241　suite of potential unimolecular reaction channels (Scheme 2). The channel-specific rate

242　coefficients are calculated with the MC-TST approach from Møller et al.[23] (Table S6 and S7). α-

243　pinene ring-opened RO$_2$ (i.e., 3-OH,8-RO$_2$) exist in both *syn* and *anti* isomers, depending on the

244　relative positions of the –OH and the -C(CH$_3$)$_2$OO groups (Scheme 2a and 2b). For the

245　experimental configuration used in this study we are unable to separate HNs derived from the *syn*

246　and *anti* ring-opened RO$_2$, and thus we experimentally infer the isomer-averaged sum of

247　unimolecular reaction rates of the precursor RO$_2$'s. For *anti* 3-OH,8-RO$_2$, the fastest unimolecular

248　pathway is calculated to be the 1,5 H-shift from C6 (1.1 s^{-1}), followed by the 1,6 H-shift from C3

249　(0.37 s^{-1}) and the endo-cyclization to C7 (0.35 s^{-1}) at 298.15 K. The remaining unimolecular

250　reactions are calculated to be very slow ($< \sim 10^{-3}$ s^{-1}). The rate of 1,5 H-shift from C6 is enhanced

251　due to stability of the nascent allylic radical. While the 1,6 H-shift from C3 also forms an allylic

252　radical, the calculated rate is slower than the 1,5 H-shift from C6, which is likely because the 1,6

253　H-shift requires a greater distortion of the ring inducing more ring-strain (Figure S5). In addition

254　to H-shift, *anti* 3-OH,8-RO$_2$ can undergo endo-cyclization to form bicyclic alkyl radical. The endo-

12

255   addition at C7 is favored over the endo-addition at C2, as the former yields a tertiary alkyl radical

256   with a six-membered ring. The calculated summed rate of unimolecular reactions of all channels

257   for *anti* 3-OH,8-RO$_2$ is 1.8 s^{-1} at 298.15 K. For *syn* 3-OH,8-RO$_2$, the dominant isomerization

258   pathway is predicted to be endo-addition to C7 (2.3 s^{-1}), followed by 1,5 H-shift from C6 (0.16 s^{-1}

259   ). Unlike *anti* 3-OH,8-RO$_2$, *syn* 3-OH,8-RO$_2$ cannot undergo a 1,6 H-shift from C3 because the

260   peroxy radical and C3-H are on opposite sides of the six-membered ring. The summed rate of

261   unimolecular reactions of *syn* 3-OH,8-RO$_2$ is 2.5 s^{-1} at 298.15 K. Assuming that *anti* and *syn* 3-

262   OH,8-RO$_2$ are initially produced in equal abundance, we find that the calculated average rate of

263   unimolecular reactions of 3-OH,8-RO$_2$ (2.1 s^{-1}) agrees with the measured value (4±2 s^{-1}), within

264   uncertainty.

265   In the β-pinene system, the ring-opened RO$_2$ (i.e., 1-OH,8-RO$_2$) only has one chiral center.

266   We do not distinguish between enantiomers, as their unimolecular reaction rate coefficients are

267   the same. We calculate that 1-OH,8-RO$_2$ primarily undergoes endo-cyclization to C7 (4.0 s^{-1}), 1,5

268   H-shift from C6 (1.4 s^{-1}), and 1,6 H-shift from C3 (0.28 s^{-1}) at 298.15 K. The summed rate of

269   unimolecular reactions of 1-OH,8-RO$_2$ (5.7 s^{-1}) agrees with the measured value (i.e., 16±5 s^{-1}),

270   within uncertainty. The calculated endo-cyclization rate coefficients of β-pinene 1-OH,8-RO$_2$ and

271   α-pinene *syn* 3-OH,8-RO$_2$ are roughly 10 times faster than that of α-pinene *anti* 3-OH,8-RO$_2$. This

272   is likely because β-pinene 1-OH,8-RO$_2$ and α-pinene *syn* 3-OH,8-RO$_2$ exhibit a hydrogen bond

273   interaction between the –OH and –OO, stabilizing the transition state (Figure S6). This option is

274   not available to the *anti* 3-OH,8-RO$_2$ as the two functional groups are on opposite sides of the ring.

275   **Reaction Products of Ring-Opened RO$_2$ under long $\tau_{bimolecular}$.** In experiments with long

276    $\tau_{bimolecular}$, we detect several stable end products that appear to arise from the unimolecular reactions.

277   For α-pinene, we observe two peaks in the chromatogram of *m/z* 332 (C$_{10}$H$_{17}$NO$_6$·CF$_3$O$^-$),

278   corresponding to the mass of organic nitrates P1 and P4-P6 (Scheme 3) produced from secondary

279   generation RO_2 (R1, R4-R6) reaction with NO. To probe the identity of compounds at m/z 332,

280   we add O_3 to the reaction chamber after photooxidation to test for the presence of C-C double

281   bonds. Both peaks at m/z 332 in GC chromatography are still present after O_3 addition (Figure S7).

282   In addition, tests are conducted through adding D_2O to the GC eluent to determine the number of

283   exchangeable H atoms (-OH and –OOH groups) in the molecules by H/D exchange reactions. The

284   H/D analysis reveals only one exchangeable H atom in $C_{10}H_{17}NO_6$. These tests suggest that the

285   compounds detected at m/z 332 are saturated with one acidic H (e.g., isomers of P1) rather than

286   unsaturated with two acidic H's (e.g., P4-P6). The lack of P4-P6 formation is likely because either

287   their precursor RO_2 (R4-R6) undergo unimolecular reactions (as discussed below and shown in

288   Scheme S4) or that P4-P6 have poor transmission efficiency through the GC.

289   A co-product of P1 from R1 reaction with NO is alkoxy radical R2. The likely fate of R2

290   is decomposition via two scission channels, both of which can lead to products sharing the same

291   chemical formula, $C_{10}H_{16}O_4$ (endoperoxide ketoaldehyde P2 and hydroxy diketone aldehyde P3

292   in Scheme 3). At long $\tau_{bimolecular}$ (i.e., 2.4 s in Figure 3), we detect one peak in the chromatogram

293   of m/z 285 ($C_{10}H_{16}O_4 \cdot CF_3O^-$). The H/D exchange analysis suggests that this peak does not have

294   any exchangeable H, implying the presence of P2, instead of P3 (has one –OH group). This

295   observation is consistent with our and earlier theoretical calculations[60] that the major

296   decomposition pathway of R2 is scission towards the –OH group to produce R3 and subsequently

297   P2 (Table S13). The assignment of P2 is further supported in that the signal from this peak is highly

298   correlated with P1, which originates from the same precursor RO_2 (i.e., R1) (Figure S8).

299   One oxidation product of the 1,6 H-shift of the hydrogen attached to C3 for α-pinene $anti$

300   3-OH,8-RO_2 is a hydroperoxide ketone ($C_{10}H_{16}O_3$, P7 in Scheme 3), generated by O_2 addition to

301   C3 in the alkyl radical and subsequent HO_2 elimination. This product is assigned to one peak in

302   the chromatogram of m/z 269 ($C_{10}H_{16}O_3 \cdot CF_3O^-$) (Figure S9), because this peak has one

303   exchangeable H, a C-C double bond, and increases with longer $\tau_{bimolecular}$ (Figure 4).

304   For β-pinene, the endo-cyclization channel is calculated to account for 70% of the RO_2

305   unimolecular reactivity based on MC-TST calculated rates. Similar to α-pinene, the endo-

306   cyclization channel produces an endoperoxide hydroxy nitrate after reaction with O_2 and NO, the

307   observed formation of which is enhanced under longer $\tau_{bimolecular}$ (Figure 4). The alkoxy radical

308   from the endo-cyclization channel (similar to R2 in Scheme 3) is calculated to primarily break the

309   carbon-carbon bond attached to the endocyclic peroxide and subsequently decompose (Scheme

310   S6).

311   **Reaction Products of Ring-Opened RO_2 under short $\tau_{bimolecular}$.** In α-pinene experiments with

312   short $\tau_{bimolecular}$, we also observe a number of stable end products (Scheme 4). We observe a CIMS

313   signal at m/z 316 ($C_{10}H_{17}NO_5 \cdot CF_3O^-$). A product with the same mass (MW 231 amu) has been

314   detected and proposed to be dihydroxy nitrate by Aschmann et al. [66] However, H/D exchange

315   analysis reveals only one acidic H in this product. One possible pathway to form the detected

316   products at m/z 316 is endo-cyclization of ring-opened hydroxy alkoxy radical (calculated earlier

317   to have an extremely low barrier [60]), followed by reaction with O_2 and NO to produce nitrate P8

318   as shown in Scheme 4. This proposed structure is further supported by the O_3 test, which suggests

319   the absence of C-C double bond in the compound. At short $\tau_{bimolecular}$, we also observe a GC peak

320   at m/z 285 ($C_{10}H_{16}O_4 \cdot CF_3O^-$), which shares the same chemical formula, but different retention time

321   as P2 produced at long $\tau_{bimolecular}$ (Figure 3). Aschmann et al. also observed a signal for a compound

322   of molecular weight 200 amu (e.g., $C_{10}H_{16}O_4$) [66] at short $\tau_{bimolecular}$. They assigned this signal to a

323   trihydroxy carbonyl. Our H/D exchange analysis reveals, however, that this product does not have

15

324   any acidic H. The lack of acidic H in $C_{10}H_{16}O_4$ is consistent with the dicarbonyl ketone ester

325   proposed by Vereecken et al. [60] (P9 shown in Scheme 4). Finally, multiple isomers are resolved at

326   *m/z* 269 ($C_{10}H_{16}O_3 \cdot CF_3O^-$, Figure S9) and all contain one exchangeable H. Previously proposed

327   structures for compounds with this mass have more than one –OH or –OOH group [66].

Potential Routes to Form Highly Oxygenated Organic Compounds. In addition to producing

329   the end products discussed above, the second-generation RO_2 (e.g., R4-R6 in Scheme 3) can

330   undergo further unimolecular reactions at enhanced rates due to their multi-functional groups

331   (hydroxy, hydroperoxy, and C-C double bond) [18-19, 67]. Several of these reactions likely lead to the

332   formation of HOMs. In Scheme 5, we show an example route to the formation of a $C_{10}H_{16}O_{10}$

333   compound, one or more species having the same chemical formula have previously been detected

334   by a NO_3^- CIMS and reaches daily maximum in the afternoon in the southeastern U.S. [68]. Peroxy

335   radical R4 can undergo a rapid OOH-OO 1,7 H-shift to produce peroxy radical R11. The rate

336   coefficient of similar H-shifts has been calculated to be on the order of 10^5 s^{-1} in other systems[67].

337   R11 can abstract the allylic H on C3 adjacent to the hydroxy group, the rate coefficient of which

338   is calculated to be 0.37 s^{-1} for a RO_2 with similar structure (α-pinene *anti* 3-OH,8-RO_2). Then,

339   following O_2 addition to C7, fast OOH-OO shift, shift of allylic H at C4, and O_2 addition to C4, a

340   peroxy radical R16 is produced. R16 can undergo 1,5 H-shift by abstracting the enolic H which

341   has been calculated in other systems to be extremely fast (~10^6 s^{-1} [69]) and produce alkyl radical

342   R17. R17 reacts with O_2, undergoes a series of fast OOH-OO shifts, abstracts the H at C4 adjacent

343   to –OOH (~ 0.1 s^{-1} in another system[70]), and finally eliminates a –OH to produce $C_{10}H_{16}O_{10}$. This

344   is just one of many plausible routes (Scheme S4 and S5) leading to the formation of HOMs. RO_2

345   with chemical composition HO-$C_{10}H_{15}$(OO)(OOH)O_2, for example, have been detected in the OH

346   oxidation of α-pinene and β-pinene [21], suggestive of fast regenerative unimolecular reactions of

347   RO_2 followed by O_2 addition, that is, RO_2 autoxidation.

348   **Yields of Hydroxy Nitrates.** Formation of HNs is an important process in atmospheric

349   photochemistry. This pathway sequesters NO_x and thus inhibits oxidant formation [71]. In this study,

350   we measure the overall yield of first generation α-pinene and β-pinene HNs ($C_{10}H_{17}NO_4$) to be

351   3.3±1.5% and 6.4±2.1%, respectively, at short $\tau_{bimolecular}$ ([NO]>1000 ppbv). The details regarding

352   the instrumental sensitivity, the effect of secondary loss and gas/particle partitioning on the

353   measured yields are discussed in SI section S5. The measured yields are much lower than those

354   estimated from structure-activity-relationship (~30%) [72]. The monoterpene RO_2, however, have

355   more complicated structures than most of the alkenes studied previously [63, 73-74]. Our values are

356   consistent with a finding of Teng et al. [63] that internal alkenes have a lower yield of hydroxy

357   nitrates than terminal alkenes with the same carbon number. Although poorly constrained in the

358   literature, perhaps the nitrate yield from cyclic β-hydroxy RO_2 + NO is also lower than their non-

359   cyclic counterparts. We estimate the nitrate branching ratio (BR_{RONO2}) of different RO_2 isomers

360   and detailed discussions are included in the SI section S6 and Table S21.

361   **The ring-opening fraction of alkyl radicals.** As we find that only the ring-opened RO_2 undergo

362   unimolecular reactions at appreciable rates, the importance of RO_2 unimolecular chemistry

363   depends critically on the yield of the ring-opened RO_2 ($Y_{ring-opened\ RO2}$). $Y_{ring-opened\ RO2}$ can be

364   calculated by Eqn. (3)

365    $Y_{ring-opened\ RO2} = BR_{OH\_add} \times BR_{OH\_less\_sub} \times BR_{ring-open}$ Eqn. (3)

366   where BR_{OH_add} represents the branching ratio of the OH chemistry proceeding via addition,

367    $BR_{OH\_less\_sub}$ represents the branching ratio of OH adding onto the less-substituted olefinic carbon,

368   and $BR_{ring-open}$ represents the branching ratio of the tertiary alkyl radical that opens the four-

17

369   membered ring. BR here is defined as the ratio of the rate constant for a particular product of a

370   reaction to the rate constant for the total set of possible products[75].

371   Early theoretical studies estimate that BR_{OH_add} is 90% based on structure-activity

372   relationships [4, 61]. The approximately 10% of the OH chemistry that proceeds via H-abstraction

373   does not lead to ring opening.

374   For the OH addition, only the addition at the less-substituted olefinic carbon (i.e., C3 in α-

375   pinene and C1 in β-pinene) leads to formation of tertiary alkyl radicals that can undergo ring

376   opening (i.e., 3-OH,2-R• for α-pinene and 1-OH,2-R• for β-pinene). Previous studies calculated

377    $BR_{OH\_less\_sub}$ as 50% and 93% for α-pinene and β-pinene, respectively[5, 61]. However, $BR_{OH\_less\_sub}$

378   is uncertain and not experimentally constrained yet. For example, the OH addition branching ratio

379   of 2-methyl 2-butene, which shares some similarity to the substitutions on α-pinene C-C double

380   bond, is 69% : 31% [63]. The uncertainties in the OH addition branching ratio will be propagated

381   into the calculated $Y_{ring-opened\ RO2}$.

382   Regarding the opening of the four-membered ring, theoretical calculations show that this

383   process is driven by the excess energy from OH addition; at room temperature, the canonical MC-

384   TST rate coefficients for this process are much too slow to compete with the O_2-addition (Table

385   S15 and Vereecken et al. [4]). Using RRKM theory at the CCSD(T)-F12a/VDZ-F12//ωB97X-D/aug-

386   cc-pVTZ level), we calculate that at atmospheric pressure and room temperature $BR_{ring-open}$ is 32%

387   and 44% for α-pinene 3-OH,2-R• and β-pinene 1-OH,2-R•, respectively (calculation details in SI

388   Section S3). These $BR_{ring-open}$ are somewhat lower than those calculated by Vereecken et al. (50%

389   and 70% for α-pinene and β-pinene, respectively)[4-5]. The calculated fractions are, however, highly

390   sensitive to the energy barrier to break the four-membered ring and the assumed energy transfer

391   per collision with bath gas (Tables S17 and S18). For example, as a sensitivity test we varied the

18

392   energy barrier to break the four-membered ring by ± 1 kcal/mol (the estimated uncertainty in the

393   calculated reaction barrier). This changes the calculated ring-opening fraction by about a factor of

394   2 in either direction for both monoterpenes. Table 1 briefly summarizes the above discussed

395   branching ratios.

396   From the measured distribution of HNs under high NO condition, it is not possible to

397   directly calculate $Y_{\text{ring-opened RO2}}$ because we do not know the nitrate branching ratio (BR_{RONO2}) for

398   all RO_2. We suggest, however, that the ratio of the yield of α-pinene ring-opened RO_2 to that of β-

399   pinene (i.e., $\frac{Yield_{\alpha-pinene\ 3-OH,8-OO}}{Yield_{\beta-pinene\ 1-OH,8-OO}}$) can be estimated from our HN measurements. As the ring-

400   opened RO_2 of both terpenes share very similar structure (i.e., tertiary RO_2 in the $-C(CH_3)_2OO$

401   group), it is reasonable to assume that these RO_2 have similar BR_{RONO2}. Following this assumption,

402    $\frac{Yield_{\alpha-pinene\ 3-OH,8-OO}}{Yield_{\beta-pinene\ 1-OH,8-OO}}$ should be similar to $\frac{Yield_{\alpha-pinene\ 3-OH,8-ONO_2}}{Yield_{\beta-pinene\ 1-OH,8-ONO_2}}$. At [NO] > 1000ppb,

403    $\frac{Yield_{\alpha-pinene\ 3-OH,8-ONO_2}}{Yield_{\beta-pinene\ 1-OH,8-ONO_2}}$ is 2.7 (i.e., $\frac{1.6\%}{0.6\%}$). Thus, we suggest $\frac{Yield_{\alpha-pinene\ 3-OH,8-OO}}{Yield_{\beta-pinene\ 1-OH,8-OO}}$ to be 2.7 - much

404   large than theoretical calculation by using Eqn. (3) (i.e., 0.39 as shown Table 1).

405   To go further, we infer the $BR_{\text{ring-open}}$ of both terpenes by making additional assumptions

406   about BR_{RONO2} and solving system of equations. If we assume that all the β-hydroxy RO_2 have the

407   same BR_{RONO2} (denoted as $BR_{RONO2,\beta-OH}$) according to Teng et al.[16] and assume that the ring-

408   opened RO_2 of both α-pinene and β-pinene have the same BR_{RONO2} (denoted as $BR_{RONO2,\text{ring-open}}$),

409   we can express the measured yields of six hydroxy nitrate isomers (α-pinene and β-pinene

410   combined) as the product of branching ratio of each step as shown below,

411    $Y_{\alpha\text{-pinene 3-OH,8-ONO2}} = BR_{OH\_add} \times BR_{add\_C3} \times BR_{\alpha\text{-pinene,ring-open}} \times BR_{RONO2,\text{ring-open}}$

412    $Y_{\alpha\text{-pinene 3-OH,2-ONO2}} = BR_{OH\_add} \times BR_{add\_C3} \times (1- BR_{\alpha\text{-pinene,ring-open}}) \times BR_{RONO2,\beta-OH}$

413    $Y_{\alpha\text{-pinene 2-OH,3-ONO2}} = BR_{OH\_add} \times (1\text{-}BR_{add\_C3}) \times BR_{RONO2,\beta\text{-OH}}$

414    $Y_{\beta\text{-pinene 1-OH,8-ONO2}} = BR_{OH\_add} \times BR_{add\_C1} \times BR_{\beta\text{-pinene,ring-open}} \times BR_{RONO2,ring\text{-open}}$

415    $Y_{\beta\text{-pinene 1-OH,2-ONO2}} = BR_{OH\_add} \times BR_{add\_C1} \times (1\text{-}BR_{\beta\text{-pinene,ring-open}}) \times BR_{RONO2,\beta\text{-OH}}$

416    $Y_{\beta\text{-pinene 2-OH,1-ONO2}} = BR_{OH\_add} \times (1\text{-}BR_{add\_C1}) \times BR_{RONO2,\beta\text{-OH}}$

417   where BR_{add_C3} and BR_{add_C1} represent the branching ratio of OH adding onto C3 and C1 in α-

418   pinene and β-pinene, respectively. BR_{OH_add} is 0.9 as discussed above. BR_{add_C3}, BR_{add_C1}, $BR_{\alpha\text{-}}$

419    $_{pinene,ring\text{-}open}$, $BR_{\beta\text{-pinene,ring-open}}$, $BR_{RONO2,\beta\text{-OH}}$, and $BR_{RONO2,ring\text{-open}}$ are unknowns. By solving the

420   system of equations (six unknowns and six equations), we find that $BR_{ring\text{-open}}$ is 97% and 34% for

421   α-pinene and β-pinene, respectively.

422   Similarly, if we assume that the ratio of BR_{RONO2} for tertiary, secondary, and primary β-

423   hydroxy RO_2 is 1.25: 1: 0.75 as suggested by Wennberg et al.[72], $BR_{ring\text{-open}}$ is found to be 97% and

424   36% for α-pinene and β-pinene, respectively (SI section S6). The discussions on the other inferred

425   parameters, such as BR_{RONO2}, can be found in the SI section S6. In summary, this analysis suggests

426   that essentially all the tertiary alkyl radicals formed in OH + α-pinene (i.e., 3-OH,2-R•) ring-open

427   while only ~1/3 of those do so for β-pinene. As the BR_{RONO2} exhibits highly complicated

428   dependence on molecular size, structure, and functionality, we place very low confidence in these

429   estimates. However, we place much higher confidence in the ratio of the yield of α-pinene ring-

430   opened RO_2 to that of β-pinene (i.e., 2.7).

431   One approach used in the literature to evaluate the ring-opening fraction has been to

432   compare the measured yields of oxidation products, such as pinonaldehyde and acetone, with the

433   theoretical yield obtained by propagating the branching ratio of each step (e.g., Scheme S7)[4]. For

434   example, using a ring-opening fraction of 50% and branching ratios of other reaction steps (SI

435   section S6), Peeters et al. calculated the pinonaldehyde yield from α-pinene photooxidation to be

436   59.5%[61]. This yield is about twice as the measured yield (27-35%)[2, 76-77] under conditions similar

437   to theoretical calculation (see SI section S6 for more discussions). Using the highly uncertain

438   branching ratios inferred above based on Wennberg et al.[72] suggested BR_{RONO2}, the implied

439   pinonaldehyde yield is 17% (2% from 3-OH,2-RO_2 and 15% from 2-OH,3-RO_2).

440   In addition to pinonaldehyde, acetone yields have also been used to estimate the ring-

441   opening fraction. Acetone has been proposed to be the major decomposition product of ring-

442   opened hydroxy alkoxy radicals (see Scheme 4 for α-pinene). However, an earlier theoretical study

443   suggested that the endo-cyclization of R1 has an extremely low barrier, which is about 3.6 kcal

444   mol^{-1} lower than that of acetone elimination[60] – consistent with the formation of the $C_{10}H_{17}NO_5$

445   hydroxy nitrates described above. Thus, the endo-cyclization easily outruns the acetone

446   elimination reaction. An alternative formation pathway for acetone has been proposed in

447   Vereecken et al.[60] Experimental evidence from this study supports this theoretically-based

448   prediction: we observe a very low yield of $C_7H_{11}NO_4$, 0.2% (assuming the same sensitivity as

449    $C_{10}H_{17}NO_4$), which is expected as a co-product of acetone elimination (Scheme S7). This yield is

450   ten times smaller than expected based on the measured acetone yield (10%)[77] and an assumed 20%

451   nitrate branching ratio (using cyclohexane as a surrogate)[78]. Thus, acetone elimination is likely

452   only a minor pathway of the ring-opened alkoxy radical and thus not a good constraint on the ring-

453   opening fraction.

Conclusions

455   Unimolecular reactions of ring-opened RO_2 in the OH oxidation of α-pinene (4±2 s^{-1}) and β-pinene

456   (16±5 s^{-1}) are shown here to outrun bimolecular chemistry in the atmosphere. While the ring-

457   opening fraction of alkyl radical remains highly uncertain, our results suggest that this fraction is

21

458 roughly a factor of three larger for α-pinene than β-pinene. This ring-opening fraction determines

459 the yield of ring-opened RO_2 formed in both α-pinene and β-pinene systems and the extent to

460 which the RO_2 unimolecular reactions occur.

461 In contrast to RO_2 bimolecular reactions with NO, the unimolecular reactions do not

462 convert NO to NO_2 and hence influence the O_3 formation. This unimolecular chemistry, currently

463 not considered in atmospheric models, may lead to an over-prediction in O_3 formation rate by

464 models[79]. On the other hand, the low rate of nitrate formation compared with estimates using

465 structure-activity relationships, may reduce the simulated loss of NO_x due to organic nitrates,

466 impacting ozone formation in the opposite direction. In addition, as shown in many reaction

467 schemes in this study, hydroxyl radical or hydroperoxyl radical are likely generated at the

468 termination step of unimolecular reactions. A detailed understanding on the sensitivity of

469 atmospheric oxidation capacity to unimolecular reactions such as these warrants further modeling

470 studies.

471 The unknown kinetics of RO_2 unimolecular reactions has been a prominent challenge to

472 unravel the exact formation mechanisms of HOMs. The fast unimolecular reactions of α-pinene

473 and β-pinene ring-opened RO_2 described here support the hypothesis that formation of HOMs via

474 autoxidation occurs for monoterpenes on relevant timescales. These HOMs are important

475 contributors to ambient monoterpene organic aerosol (OA), suggested as the largest source of

476 summertime OA in the southeastern U.S.[7, 12].

477 Finally, the *ab initio* calculations, together with the detection of unimolecular reaction

478 products, imply that the unimolecular reactions of ring-opened RO_2 are enhanced by the presence

479 of C-C double bond and the hydroxy group. In light of this, it is likely that RO_2 from other

480   monoterpene species, such as limonene, terpinolene, and myrcene, also undergo similar fast

481   unimolecular reactions and deserve further study.

23

ASSOCIATED CONTENT

Supporting Information

Additional information on the peak identification of α-pinene and β-pinene hydroxy nitrates, mathematical derivations to show the relationship between the (ring-opened HN):(ring-retained HNs) ratio and RO_2 bimolecular and unimolecular lifetimes, calculation of $\tau_{bimolecular}$, computational approach, kinetic box model to calculate the rate of unimolecular reactions, discussions of yields of α-pinene and β-pinene hydroxy nitrates, discussions of uncertainties associated with the branching ratios, and discussions of nitrate branching ratio.

Output files of all calculations including the xyz-geometries can be found online at: https://sid.erda.dk/sharelink/hYtUUanavY

ACKNOWLEDGMENTS

AUTHOR INFORMATION

Corresponding Authors

* E-mail: luxu@caltech.edu

* E-mail: wennberg@caltech.edu

* E-mail: hgk@chem.ku.dk

24

503   **ORCID**

504   Lu Xu: 0000-0002-0021-9876

505   Kristian H. Møller: 0000-0001-8070-8516

506   John D. Crounse: 0000-0001-5443-729X

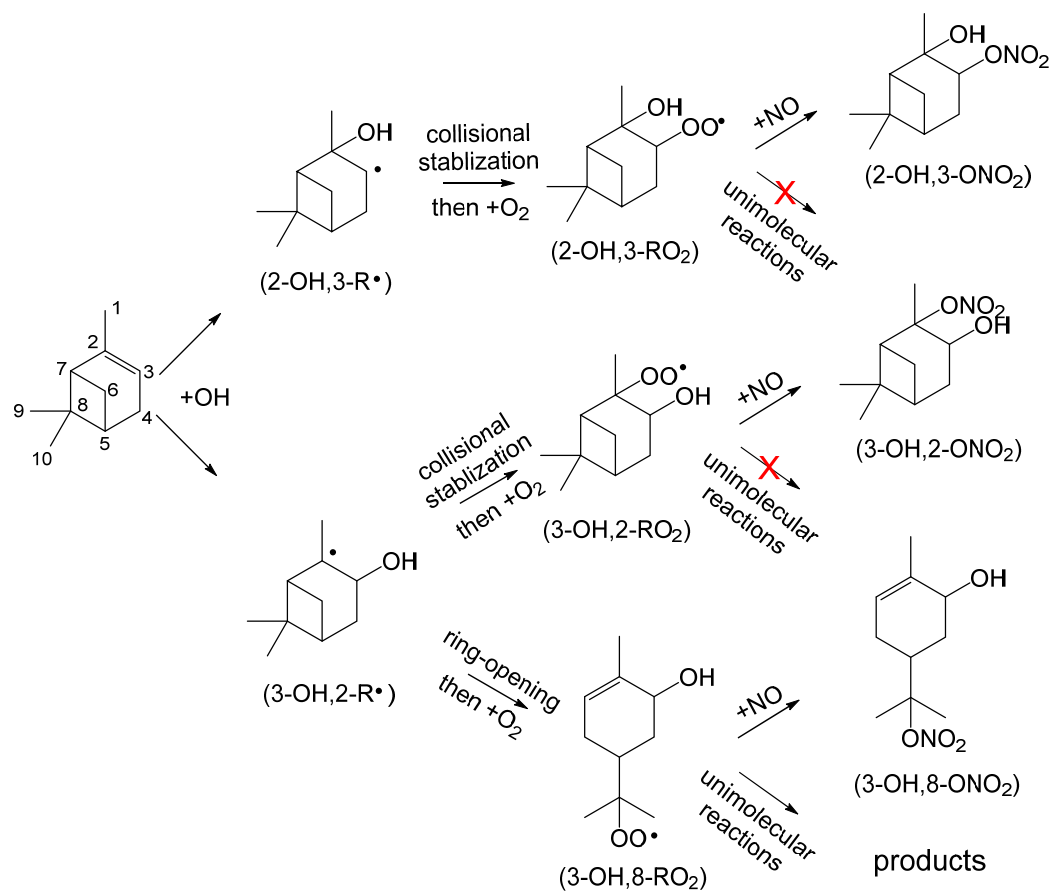507   Rasmus V. Otkjær: 0000-0002-6094-1828

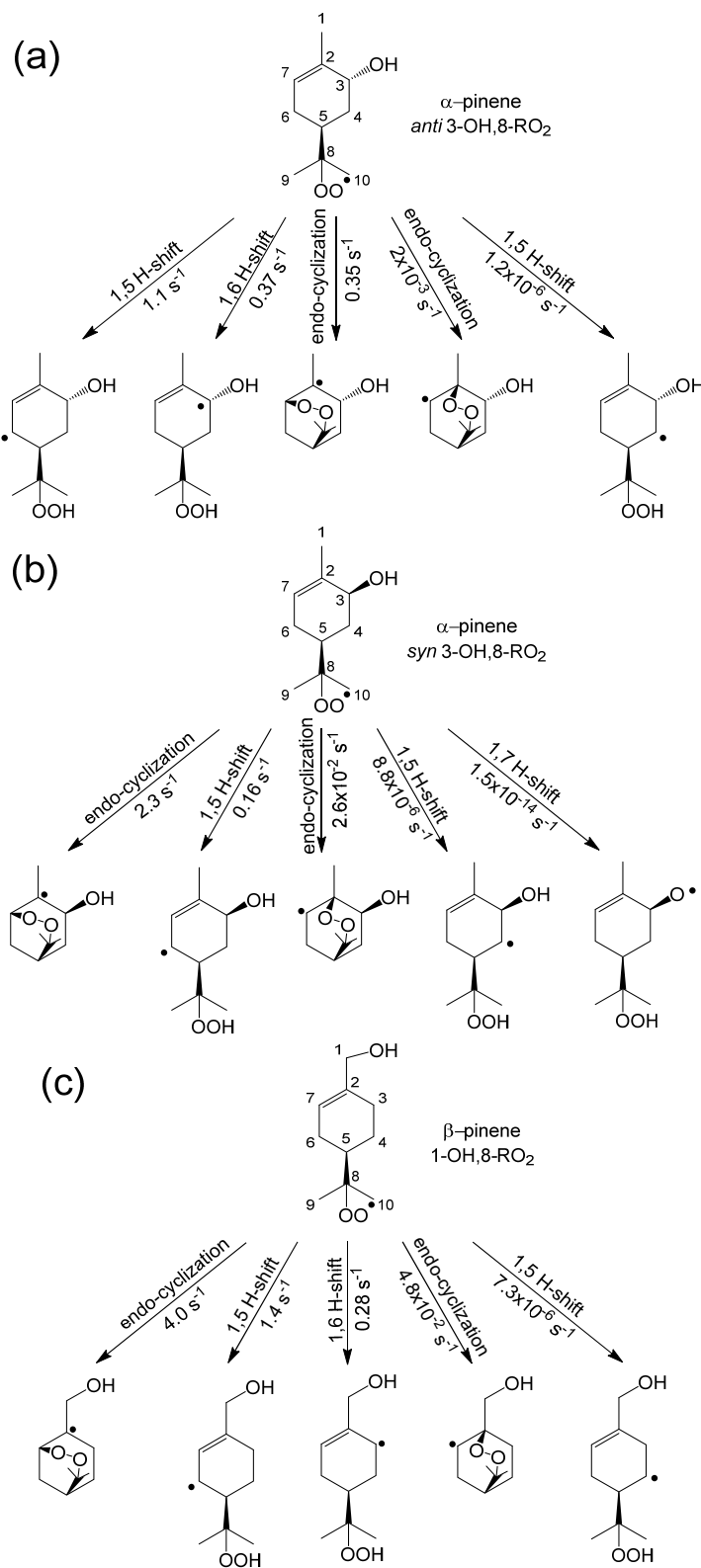508   Henrik G. Kjaergaard: 0000-0002-7275-8297

509   Paul O. Wennberg: 0000-0002-6126-3854

510   Notes: the authors declare no competing financial interest.

511

25

512

513 Scheme 1. The simplified oxidation mechanism of α-pinene. Each structural isomer of RO_2 and
514 hydroxy nitrate has multiple stereoisomers, which are shown in Scheme S2. The $RO+NO_2$
515 produced from RO_2+NO are not included in the scheme to improve clarity.

1
2
3
4
5
6
7
8
9
10
11
12
13
14
15
16
17
18
19 516
20
21
22
23
24
25
26
27
28
29
30
31
32
33
34
35 517
36
37
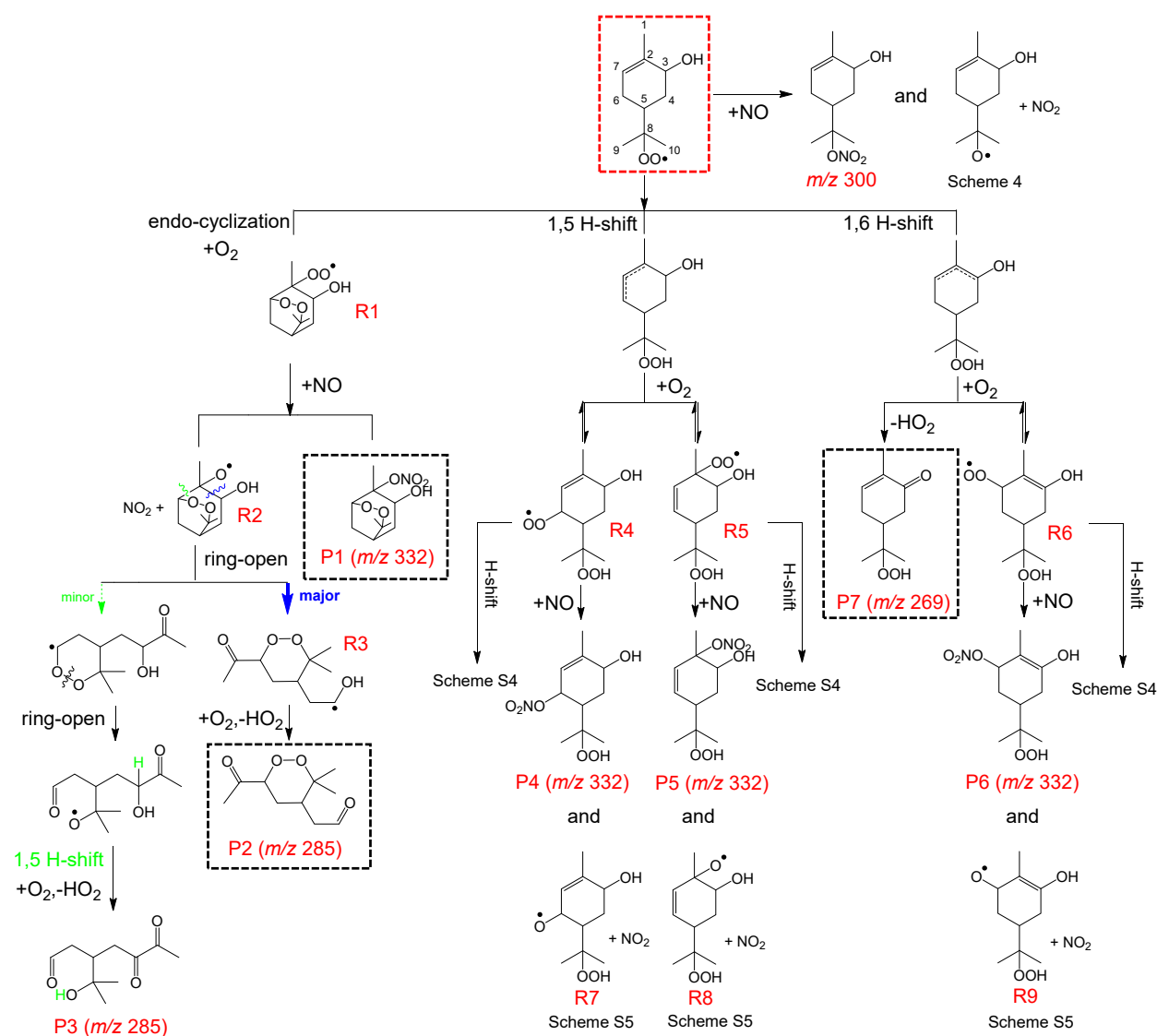38
39
40
41
42
43
44
45
46
47
48
49
50
51
52 518
53 519   Scheme 2. Unimolecular reaction channels for (a) α-pinene *anti* 3-OH,8-RO$_2$; (b) α-pinene *syn* 3-
54 520   OH,8-RO$_2$ and (c) β-pinene 1-OH,8-RO$_2$. Rate coefficients are calculated with the MC-TST
55 521   approach by Møller et al. [23] at 298.15 K.
56
57
58   27
59
60

Scheme 3. The unimolecular reaction products of α-pinene 3-OH,8-RO₂ (shown in red box). The stereoisomers are not distinguished in this scheme. The 1,6 H-shift only occurs for *anti* 3-OH,8-RO₂. Observed species are shown in black boxes. The *m/z* listed below observed species are for the complex with CF₃O⁻ (molecular mass + 85).

528
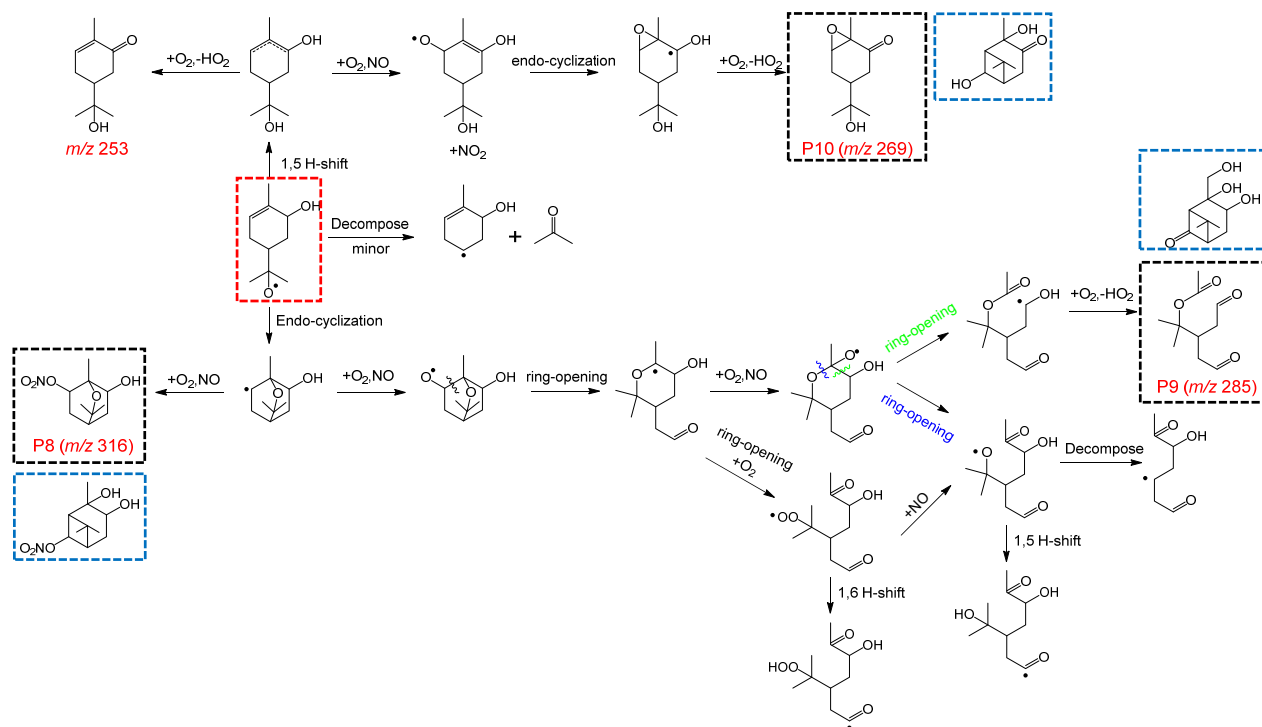
Scheme 4. Speculations on the reactions of α-pinene 3-OH,8-RO alkoxy radical (shown in red box) at short $\tau_{bimolecular}$. The *m/z* listed below observed species are for the complex with CF_3O^- (molecular mass + 85). Species having molecular weight consistent with observed signals are shown in black box. The products proposed by Aschmann et al. [66] are shown in blue boxes. NO_2 produced from RO_2+NO is not shown in the figure.
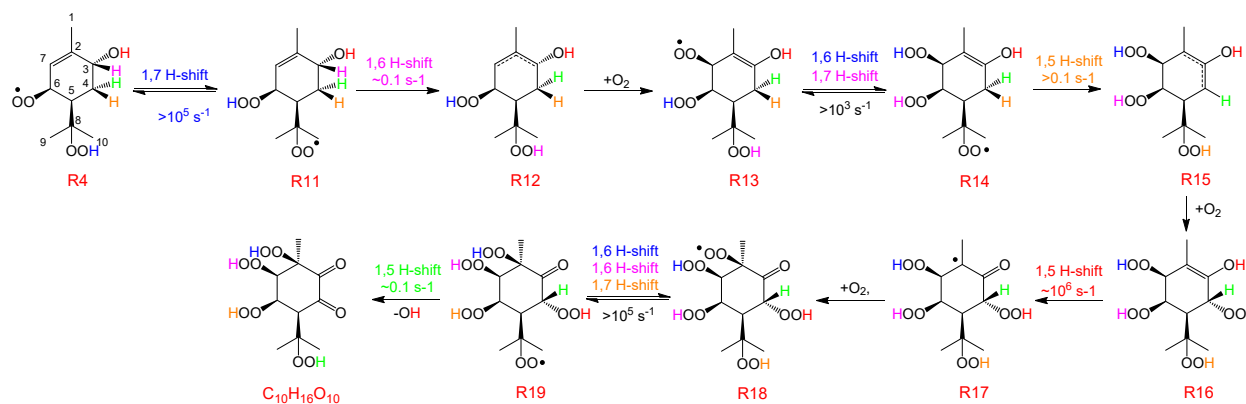
534

535 Scheme 5. An example pathway from α-pinene ring-opened RO₂ leading to the production of
536 highly oxygenated molecules. Unimolecular rate coefficients estimated from similar H-shifts at
537 298.15 K.

538
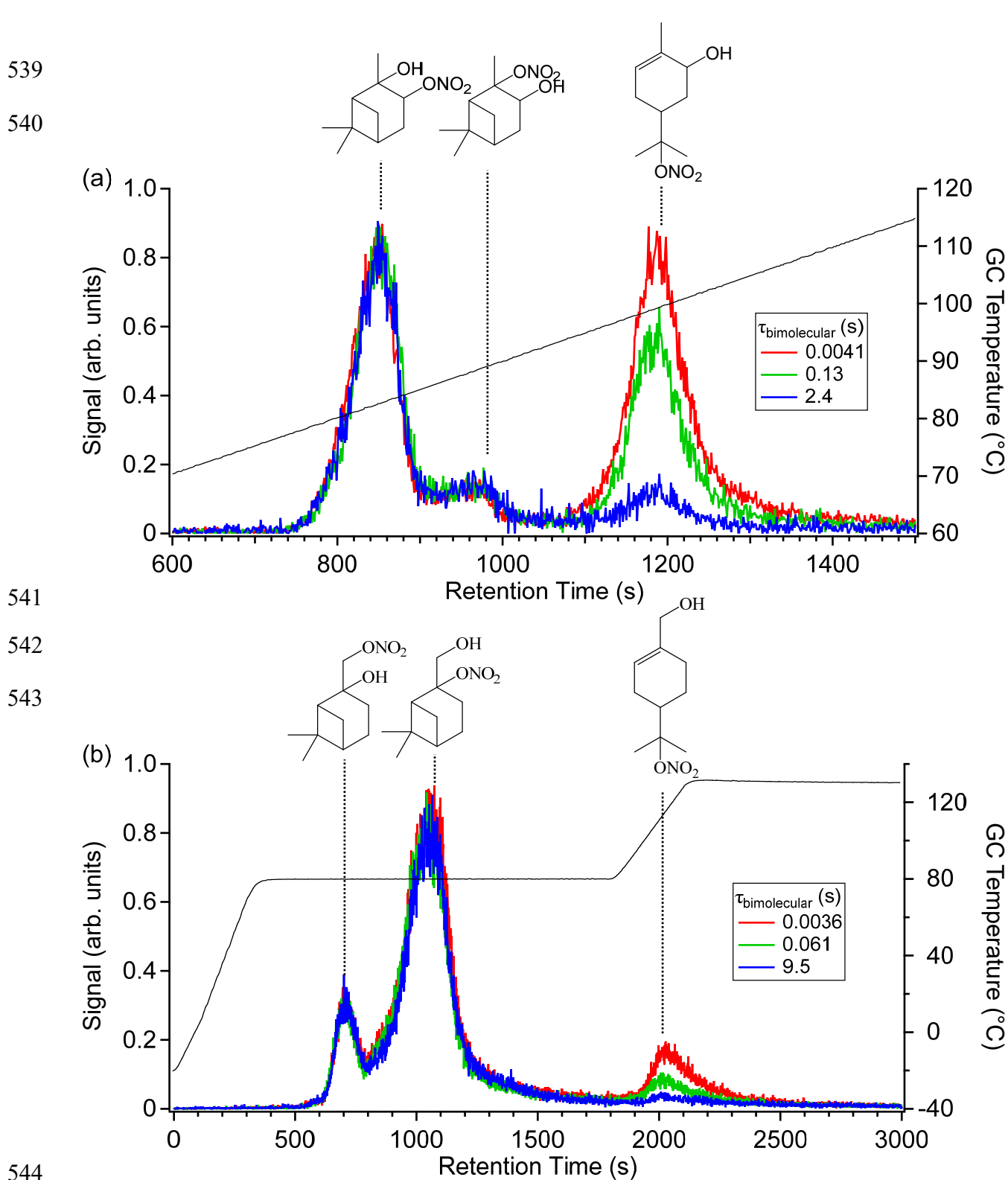
Figure 1. Chromatograms of hydroxy nitrates of (a) α-pinene and (b) β-pinene. The structural assignment of GC peaks is discussed in the SI section S1. In each panel, the GC chromatograms for three different RO_2 bimolecular lifetimes ($\tau_{bimolecular}$) are shown. The signals are scaled to match the magnitude of the ring-retained hydroxy nitrates. The black solid line shows the GC temperature.
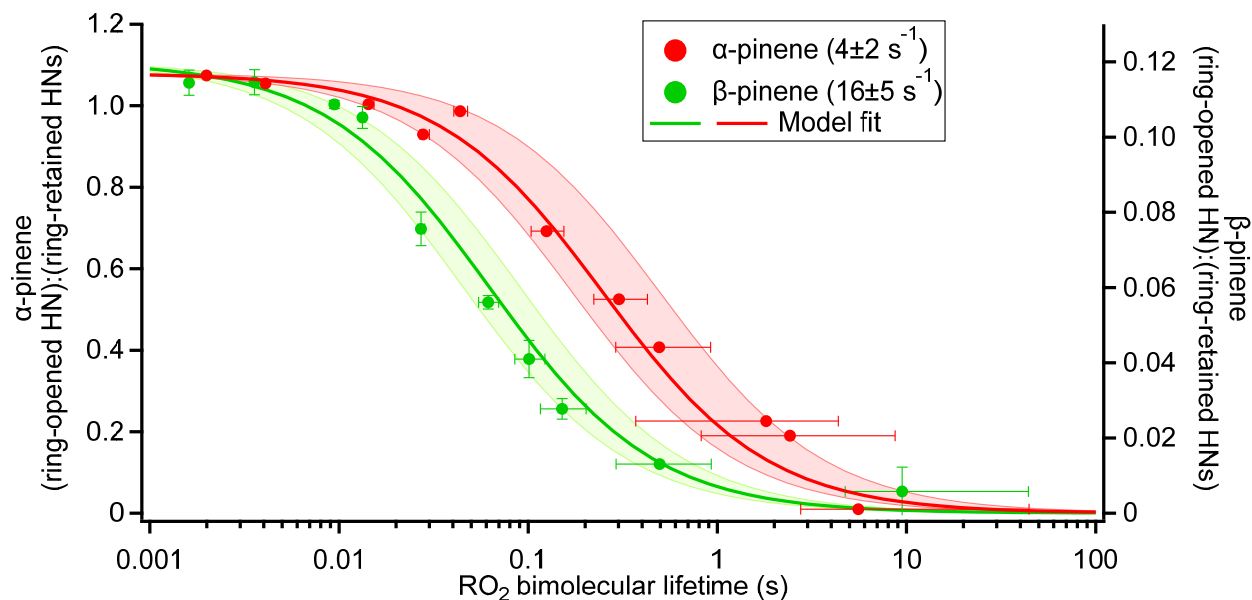
Figure 2. Ratio of ring-opened HN to ring-retained HNs of α-pinene and β-pinene as a function of RO_2 bimolecular lifetime. The uncertainty in RO_2 bimolecular lifetime is represented by the range from the beginning to the end of the photooxidation period. The solid line represents the experimentally determined average rate coefficient of unimolecular reactions of the ring-opened RO_2s. The shaded regions represent the range of uncertainty in the rate coefficients of unimolecular reactions.
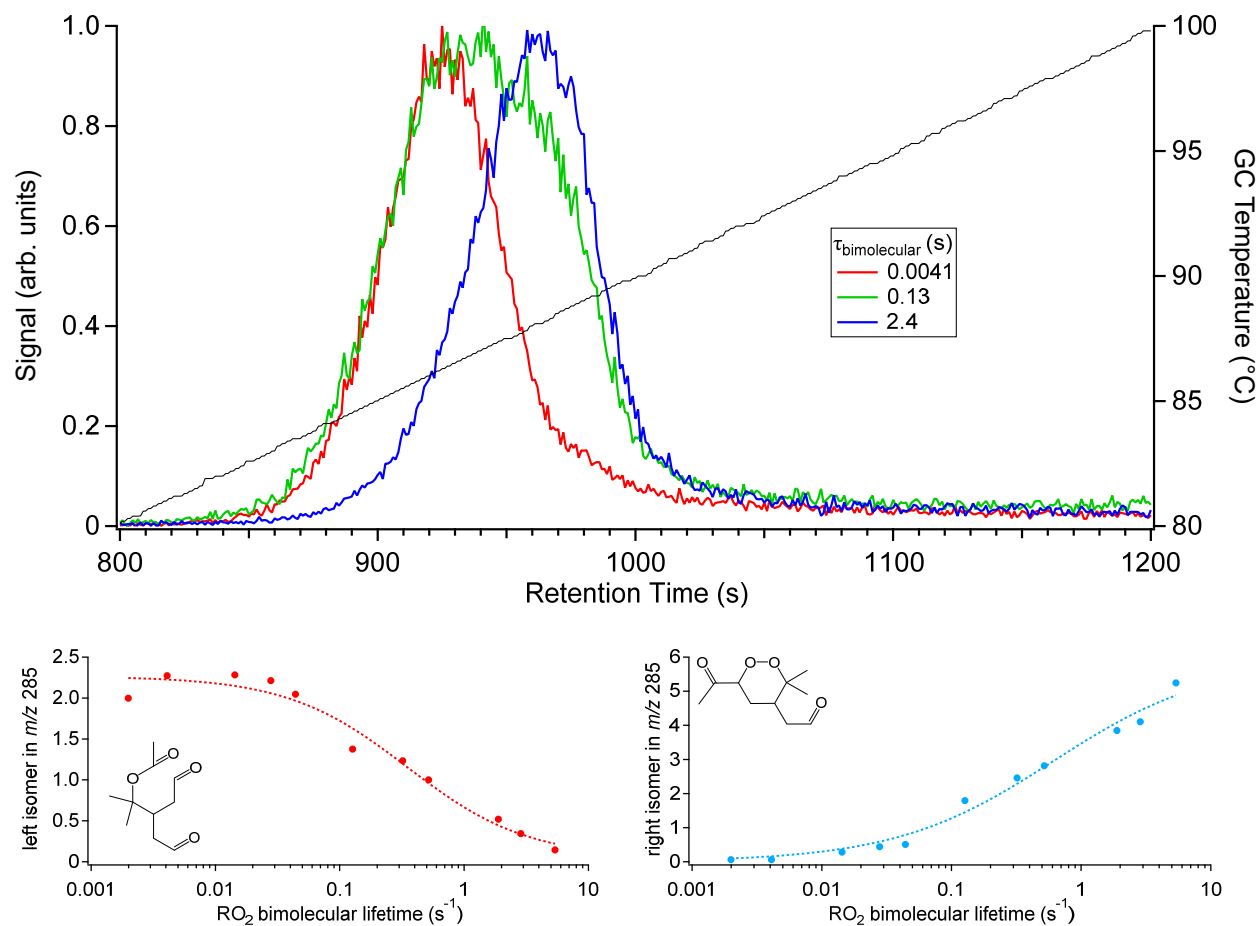
Figure 3. (Top) GC chromatograms of *m/z* 285 in α-pinene photooxidation experiments under different $\tau_{bimolecular}$. The signal is scaled by that of ring-retained HNs. H/D exchange analysis reveals that neither compound have acidic H. The proposed structures and the abundances of both peaks as a function of $\tau_{bimolecular}$ are shown in the bottom two panels.
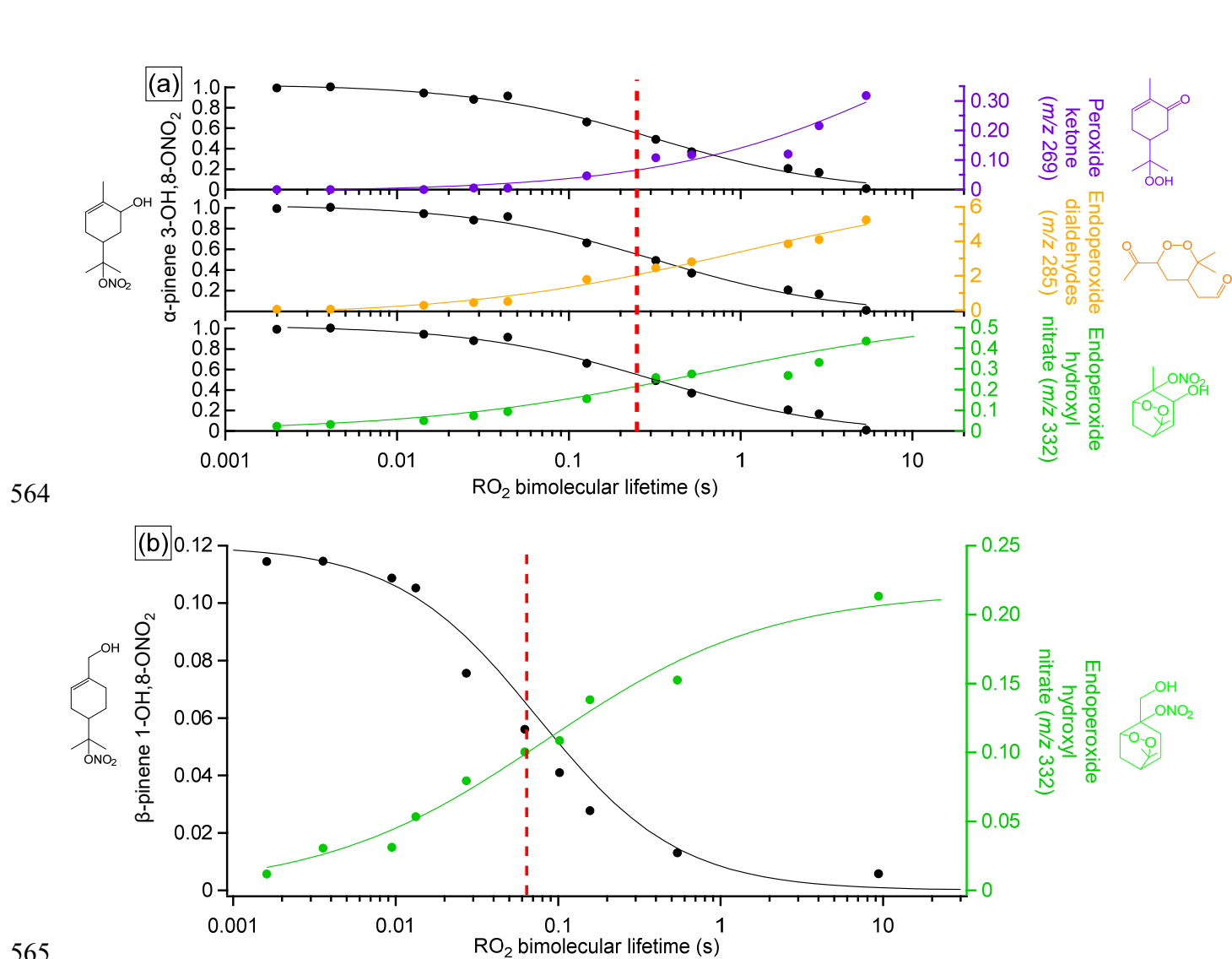
Figure 4. End products from unimolecular reactions of (a) α-pinene and (b) β-pinene as a function of RO₂ bimolecular lifetime. Data are normalized by the abundance of ring-retained hydroxy nitrates. The red dashed line indicates the unimolecular lifetime of ring-opened RO₂ at 296 K.

570   Table 1. The theoretically calculated yields of ring-opened RO_2 and the branching ratios along its

571   formation pathway of both α-pinene and β-pinene.

Compound	Reference	BR_{OH_add}[a]	$BR_{OH\_less-sub}$[b]	$BR_{ring-open}$[c]	$Yield_{ring-opened\ RO2}$[d,e]
α-pinene	Vereecken et al. (2000)[4]	0.9	0.5	0.5	0.23
	This work	-	-	0.32[f]	-
β-pinene	Vereecken et al. (2012)[5]	0.9	0.93	0.7	0.59
	This work	-	-	0.44	-

572   [a]BR_{OH_add} represents the branching ratio that terpene+OH proceeds via addition to the double bond.

573   [b]$BR_{OH\_less\_sub}$ represents the branching ratio that OH adds to the less-substituted olefinic carbon

574   (i.e., C3 and C1 in α-pinene and β-pinene, respectively).

575   [c]$BR_{ring-open}$ represents the ring-opening fraction of the activated tertiary alkyl radical.

576   [d]$Yield_{ring-opened\ RO2}$ represents that the yield of ring-opened RO_2. $Yield_{ring-opened\ RO2} = BR_{OH\_add} \times$

577    $BR_{OH\_less-sub} \times BR_{ring-open}$.

578   [e]The ratio of α-pinene $Yield_{ring-opened\ RO2}$ relative to that of β-pinene is 0.39 based on studies of

579   Vereecken et al. However, a ratio of 2.7 is derived from our measured yield of ring-opened

580   hydroxy nitrate and an assumption that the nitrate branching ratio of ring-opened RO_2 is the same

581   for both terpenes.

582   [f]α-pinene ring-opened RO_2 has two isomers, *syn* and *anti*. The calculated $BR_{ring-open}$ only differs by

583   0.02 between the two isomers (shown in Table S15). Here we report the average value. The

584   calculated values are highly sensitive to the energy barrier to break the four-membered ring and

585   the energy transfer per collision with bath gas (Tables S17 and S18).

References

1.   Guenther, A.; Jiang, X.; Heald, C. L.; Sakulyanontvittaya, T.; Duhl, T.; Emmons, L. K.; Wang, X. The Model of Emissions of Gases and Aerosols from Nature Version 2.1 (Megan2.1): An Extended and Updated Framework for Modeling Biogenic Emissions. *Geosci. Model Dev.* **2012,** *5*, 1471-1492.

2.   Eddingsaas, N. C.; Loza, C. L.; Yee, L. D.; Seinfeld, J. H.; Wennberg, P. O. A-Pinene Photooxidation under Controlled Chemical Conditions – Part 1: Gas-Phase Composition in Low- and High-Nox Environments. *Atmos. Chem. Phys.* **2012,** *12*, 6489-6504.

3.   Lee, A.; Goldstein, A. H.; Keywood, M. D.; Gao, S.; Varutbangkul, V.; Bahreini, R.; Ng, N. L.; Flagan, R. C.; Seinfeld, J. H. Gas-Phase Products and Secondary Aerosol Yields from the Ozonolysis of Ten Different Terpenes. *J. Geophys. Res. - Atmos* **2006,** *111*.

4.   Vereecken, L.; Peeters, J. Theoretical Study of the Formation of Acetone in the Oh-Initiated Atmospheric Oxidation of A-Pinene. *J. Phys. Chem. A* **2000,** *104*, 11140-11146.

5.   Vereecken, L.; Peeters, J. A Theoretical Study of the Oh-Initiated Gas-Phase Oxidation Mechanism of B-Pinene (C10h16): First Generation Products. *Phys. Chem. Chem. Phys.* **2012,** *14*, 3802-3815.

6.   Yu, J.; Cocker, D. R.; Griffin, R. J.; Flagan, R. C.; Seinfeld, J. H. Gas-Phase Ozone Oxidation of Monoterpenes: Gaseous and Particulate Products. *J. Atmos. Chem.* **1999,** *34*, 207-258.

7.   Zhang, H.; Yee, L. D.; Lee, B. H.; Curtis, M. P.; Worton, D. R.; Isaacman-VanWertz, G.; Offenberg, J. H.; Lewandowski, M.; Kleindienst, T. E.; Beaver, M. R., et al. Monoterpenes Are the Largest Source of Summertime Organic Aerosol in the Southeastern United States. *Proc. Natl. Acad. Sci. U. S. A* **2018,** *115*, 2038-2043.

8.   Ng, N. L.; Brown, S. S.; Archibald, A. T.; Atlas, E.; Cohen, R. C.; Crowley, J. N.; Day, D. A.; Donahue, N. M.; Fry, J. L.; Fuchs, H., et al. Nitrate Radicals and Biogenic Volatile Organic Compounds: Oxidation, Mechanisms, and Organic Aerosol. *Atmos. Chem. Phys.* **2017,** *17*, 2103-2162.

9.   Ehn, M.; Thornton, J. A.; Kleist, E.; Sipila, M.; Junninen, H.; Pullinen, I.; Springer, M.; Rubach, F.; Tillmann, R.; Lee, B., et al. A Large Source of Low-Volatility Secondary Organic Aerosol. *Nature* **2014,** *506*, 476-479.

10.   Pye, H. O. T.; Chan, A. W. H.; Barkley, M. P.; Seinfeld, J. H. Global Modeling of Organic Aerosol: The Importance of Reactive Nitrogen (Nox and No3). *Atmos. Chem. Phys.* **2010,** *10*, 11261-11276.

11.   Kanakidou, M.; Seinfeld, J. H.; Pandis, S. N.; Barnes, I.; Dentener, F. J.; Facchini, M. C.; Van Dingenen, R.; Ervens, B.; Nenes, A.; Nielsen, C. J., et al. Organic Aerosol and Global Climate Modelling: A Review. *Atmos. Chem. Phys.* **2005,** *5*, 1053-1123.

12.   Xu, L.; Pye, H. O. T.; He, J.; Chen, Y.; Murphy, B. N.; Ng, N. L. Experimental and Model Estimates of the Contributions from Biogenic Monoterpenes and Sesquiterpenes to Secondary Organic Aerosol in the Southeastern United States. *Atmos. Chem. Phys.* **2018,** *18*, 12613-12637.

13.   Isaacman-VanWertz, G.; Massoli, P.; O'Brien, R.; Lim, C.; Franklin, J. P.; Moss, J. A.; Hunter, J. F.; Nowak, J. B.; Canagaratna, M. R.; Misztal, P. K., et al. Chemical Evolution of Atmospheric Organic Carbon over Multiple Generations of Oxidation. *Nat. Chem.* **2018,** *10*, 462-468.

629   14.   Kroll, J. H.; Seinfeld, J. H. Chemistry of Secondary Organic Aerosol: Formation and
630   Evolution of Low-Volatility Organics in the Atmosphere. *Atmospheric Environ.* **2008,** *42*, 3593-
631   3624.
632   15.   Orlando, J. J.; Tyndall, G. S. Laboratory Studies of Organic Peroxy Radical Chemistry: An
633   Overview with Emphasis on Recent Issues of Atmospheric Significance. *Chem. Soc. Rev.* **2012,**
634   *41*, 6294-6317.
635   16.   Teng, A. P.; Crounse, J. D.; Wennberg, P. O. Isoprene Peroxy Radical Dynamics. *J. Am.*
636   *Chem. Soc.* **2017,** *139*, 5367-5377.
637   17.   Peeters, J.; Nguyen, T. L.; Vereecken, L. Hox Radical Regeneration in the Oxidation of
638   Isoprene. *Phys. Chem. Chem. Phys.* **2009,** *11*, 5935-5939.
639   18.   Praske, E.; Otkjær, R. V.; Crounse, J. D.; Hethcox, J. C.; Stoltz, B. M.; Kjaergaard, H. G.;
640   Wennberg, P. O. Atmospheric Autoxidation Is Increasingly Important in Urban and Suburban
641   North America. *Proc. Natl. Acad. Sci. U. S. A* **2018,** *115*, 64-69.
642   19.   Crounse, J. D.; Nielsen, L. B.; Jørgensen, S.; Kjaergaard, H. G.; Wennberg, P. O.
643   Autoxidation of Organic Compounds in the Atmosphere. *J. Phys. Chem. Lett* **2013,** *4*, 3513-3520.
644   20.   Vereecken, L.; Peeters, J. Nontraditional (Per)Oxy Ring-Closure Paths in the Atmospheric
645   Oxidation of Isoprene and Monoterpenes. *J. Phys. Chem. A* **2004,** *108*, 5197-5204.
646   21.   Berndt, T.; Richters, S.; Jokinen, T.; Hyttinen, N.; Kurtén, T.; Otkjær, R. V.; Kjaergaard,
647   H. G.; Stratmann, F.; Herrmann, H.; Sipilä, M., et al. Hydroxyl Radical-Induced Formation of
648   Highly Oxidized Organic Compounds. *Nat. Commun.* **2016,** *7*, 13677.
649   22.   Zhao, Y.; Thornton, J. A.; Pye, H. O. T. Quantitative Constraints on Autoxidation and
650   Dimer Formation from Direct Probing of Monoterpene-Derived Peroxy Radical Chemistry. *Proc.*
651   *Natl. Acad. Sci. U. S. A* **2018,** *115*, 12142-12147.
652   23.   Møller, K. H.; Otkjær, R. V.; Hyttinen, N.; Kurtén, T.; Kjaergaard, H. G. Cost-Effective
653   Implementation of Multiconformer Transition State Theory for Peroxy Radical Hydrogen Shift
654   Reactions. *J. Phys. Chem. A* **2016,** *120*, 10072-10087.
655   24.   Vereecken, L.; Peeters, J. The 1,5-H-Shift in 1-Butoxy: A Case Study in the Rigorous
656   Implementation of Transition State Theory for a Multirotamer System. *J. Chem. Phys.* **2003,** *119*,
657   5159-5170.
658   25.   Sharpe, S. W.; Johnson, T. J.; Sams, R. L.; Chu, P. M.; Rhoderick, G. C.; Johnson, P. A.
659   Gas-Phase Databases for Quantitative Infrared Spectroscopy. *Appl. Spectrosc.* **2004,** *58*, 1452-
660   1461.
661   26.   Taylor, W. D.; Allston, T. D.; Moscato, M. J.; Fazekas, G. B.; Kozlowski, R.; Takacs, G.
662   A. Atmospheric Photo-Dissociation Lifetimes for Nitromethane, Methyl Nitrite, and Methyl
663   Nitrate. *Int. J. Chem. Kinet.* **1980,** *12*, 231-240.
664   27.   Vasquez, K. T.; Allen, H. M.; Crounse, J. D.; Praske, E.; Xu, L.; Noelscher, A. C.;
665   Wennberg, P. O. Low-Pressure Gas Chromatography with Chemical Ionization Mass
666   Spectrometry for Quantification of Multifunctional Organic Compounds in the Atmosphere.
667   *Atmos. Meas. Tech.* **2018,** *11*, 6815-6832.
668   28.   Jenkin, M. E.; Saunders, S. M.; Pilling, M. J. The Tropospheric Degradation of Volatile
669   Organic Compounds: A Protocol for Mechanism Development. *Atmospheric Environ.* **1997,** *31*,
670   81-104.
671   29.   Saunders, S. M.; Jenkin, M. E.; Derwent, R. G.; Pilling, M. J. Protocol for the Development
672   of the Master Chemical Mechanism, Mcm V3 (Part a): Tropospheric Degradation of Non-
673   Aromatic Volatile Organic Compounds. *Atmos. Chem. Phys.* **2003,** *3*, 161-180.

37

674   30.   Crounse, J. D.; Paulot, F.; Kjaergaard, H. G.; Wennberg, P. O. Peroxy Radical
675   Isomerization in the Oxidation of Isoprene. *Phys. Chem. Chem. Phys.* **2011,** *13*, 13607-13613.
676   31.   Werner, H.-J.; Knizia, G.; Manby, F. R. Explicitly Correlated Coupled Cluster Methods
677   with Pair-Specific Geminals. *Mol. Phys.* **2011,** *109*, 407-417.
678   32.   Halgren, T. A. Mmff Vii. Characterization of Mmff94, Mmff94s, and Other Widely
679   Available Force Fields for Conformational Energies and for Intermolecular-Interaction Energies
680   and Geometries. *J. Comput. Chem.* **1999,** *20*, 730-748.
681   33.   Halgren, T. A. Merck Molecular Force Field. V. Extension of Mmff94 Using Experimental
682   Data, Additional Computational Data, and Empirical Rules. *J. Comput. Chem.* **1996,** *17*, 616-641.
683   34.   Halgren, T. A.; Nachbar, R. B. Merck Molecular Force Field. Iv. Conformational Energies
684   and Geometries for Mmff94. *J. Comput. Chem.* **1996,** *17*, 587-615.
685   35.   Halgren, T. A. Merck Molecular Force Field. Iii. Molecular Geometries and Vibrational
686   Frequencies for Mmff94. *J. Comput. Chem.* **1996,** *17*, 553-586.
687   36.   Halgren, T. A. Merck Molecular Force Field. Ii. Mmff94 Van Der Waals and Electrostatic
688   Parameters for Intermolecular Interactions. *J. Comput. Chem.* **1996,** *17*, 520-552.
689   37.   Halgren, T. A. Merck Molecular Force Field. I. Basis, Form, Scope, Parameterization, and
690   Performance of Mmff94. *J. Comput. Chem.* **1996,** *17*, 490-519.
691   38.   *Spartan'16*, Wavefunction, Inc., Irvine, CA.
692   39.   Frisch, M. J.; Trucks, G. W.; Schlegel, H. B.; Scuseria, G. E.; Robb, M. A.; Cheeseman, J.
693   R.; Scalmani, G.; Barone, V.; Petersson, G. A.; Nakatsuji, H., et al. *Gaussian 16 Rev. A.03*,
694   Wallingford, CT, 2016.
695   40.   Becke, A. D. Density‐Functional Thermochemistry. Iii. The Role of Exact Exchange. *J.
696   Chem. Phys.* **1993,** *98*, 5648-5652.
697   41.   Lee, C.; Yang, W.; Parr, R. G. Development of the Colle-Salvetti Correlation-Energy
698   Formula into a Functional of the Electron Density. *Phys. Rev. B* **1988,** *37*, 785-789.
699   42.   Hehre, W. J.; Ditchfield, R.; Pople, J. A. Self—Consistent Molecular Orbital Methods. Xii.
700   Further Extensions of Gaussian—Type Basis Sets for Use in Molecular Orbital Studies of Organic
701   Molecules. *J. Chem. Phys.* **1972,** *56*, 2257-2261.
702   43.   Clark, T.; Chandrasekhar, J.; Spitznagel, G. W.; Schleyer, P. V. R. Efficient Diffuse
703   Function-Augmented Basis Sets for Anion Calculations. Iii. The 3-21+G Basis Set for First-Row
704   Elements, Li–F. *J. Comput. Chem.* **1983,** *4*, 294-301.
705   44.   Frisch, M. J.; Pople, J. A.; Binkley, J. S. Self‐Consistent Molecular Orbital Methods 25.
706   Supplementary Functions for Gaussian Basis Sets. *J. Chem. Phys.* **1984,** *80*, 3265-3269.
707   45.   Chai, J.-D.; Head-Gordon, M. Long-Range Corrected Hybrid Density Functionals with
708   Damped Atom-Atom Dispersion Corrections. *Phys. Chem. Chem. Phys.* **2008,** *10*, 6615-6620.
709   46.   Dunning Jr., T. H. Gaussian Basis Sets for Use in Correlated Molecular Calculations. I.
710   The Atoms Boron through Neon and Hydrogen. *J. Chem. Phys.* **1989,** *90*, 1007-1023.
711   47.   Kendall, R. A.; Dunning Jr., T. H.; Harrison, R. J. Electron Affinities of the First‐Row
712   Atoms Revisited. Systematic Basis Sets and Wave Functions. *J. Chem. Phys.* **1992,** *96*, 6796-6806.
713   48.   Adler, T. B.; Knizia, G.; Werner, H.-J. A Simple and Efficient Ccsd(T)-F12 Approximation.
714   *Acc. Chem. Res.* **2007,** *127*, 221106.
715   49.   Knizia, G.; Adler, T. B.; Werner, H.-J. Simplified Ccsd(T)-F12 Methods: Theory and
716   Benchmarks. *J. Chem. Phys.* **2009,** *130*, 054104.
717   50.   Peterson, K. A.; Adler, T. B.; Werner, H.-J. Systematically Convergent Basis Sets for
718   Explicitly Correlated Wavefunctions: The Atoms H, He, B–Ne, and Al–Ar. *J. Chem. Phys.* **2008,**
719   *128*, 084102.
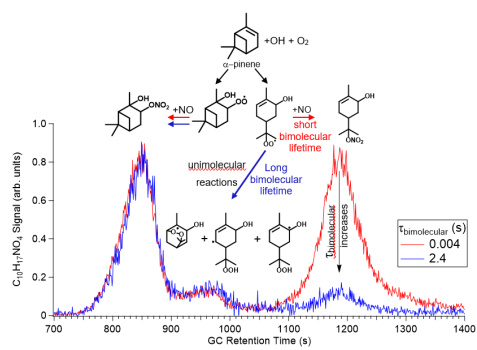
38

720   51.   Watts, J. D.; Gauss, J.; Bartlett, R. J. Coupled‐Cluster Methods with Noniterative Triple
721   Excitations for Restricted Open‐Shell Hartree–Fock and Other General Single Determinant
722   Reference Functions. Energies and Analytical Gradients. *J. Chem. Phys.* **1993,** *98*, 8718-8733.
723   52.   Werner, H.-J.; Knizia, G.; R. Manby, F. Explicitly Correlated Coupled Cluster Methods
724   with Pair-Specific Geminals. *Mol. Phys.* **2011,** *109*, 407-417.
725   53.   Werner, H.-J.; Knowles, P. J.; Knizia, G.; Manby, F. R.; Schütz, M. Molpro: A General-
726   Purpose Quantum Chemistry Program Package. *Wiley Interdiscip. Rev. Comput. Mol. Sci.* **2012,**
727   *2*, 242-253.
728   54.   Werner, H.-J.; Knowles, P. J.; Knizia, G.; Manby, F. R.; Schütz, M.; Celani, P.; Györffy,
729   W.; Kats, D.; Korona, T.; Lindh, R., et al. *Molpro, Version 2012.1, a Package of Ab Initio
730   Programs*, 2012.
731   55.   Møller, K. H.; Bates, K. H.; Kjaergaard, H. G. The Importance of Peroxy Radical Hydrogen
732   Shift Reactions in Atmospheric Isoprene Oxidation. *J. Phys. Chem. A* **2019**.
733   56.   Matlab R2016b.
734   57.   Eckart, C. The Penetration of a Potential Barrier by Electrons. *Phys. Rev.* **1930,** *35*, 1303-
735   1309.
736   58.   Glowacki, D. R.; Liang, C.-H.; Morley, C.; Pilling, M. J.; Robertson, S. H. Mesmer: An
737   Open-Source Master Equation Solver for Multi-Energy Well Reactions. *J. Phys. Chem. A* **2012,**
738   *116*, 9545-9560.
739   59.   Otkjær, R. V.; Jakobsen, H. H.; Tram, C. M.; Kjaergaard, H. G. Calculated Hydrogen Shift
740   Rate Constants in Substituted Alkyl Peroxy Radicals. *J. Phys. Chem. A* **2018,** *122*, 8665-8673.
741   60.   Vereecken, L.; Muller, J. F.; Peeters, J. Low-Volatility Poly-Oxygenates in the Oh-Initiated
742   Atmospheric Oxidation of A-Pinene: Impact of Non-Traditional Peroxyl Radical Chemistry. *Phys.
743   Chem. Chem. Phys.* **2007,** *9*, 5241-5248.
744   61.   Peeters, J.; Vereecken, L.; Fantechi, G. The Detailed Mechanism of the Oh-Initiated
745   Atmospheric Oxidation of A-Pinene: A Theoretical Study. *Phys. Chem. Chem. Phys.* **2001,** *3*,
746   5489-5504.
747   62.   Kurtén, T.; Møller, K. H.; Nguyen, T. B.; Schwantes, R. H.; Misztal, P. K.; Su, L.;
748   Wennberg, P. O.; Fry, J. L.; Kjaergaard, H. G. Alkoxy Radical Bond Scissions Explain the
749   Anomalously Low Secondary Organic Aerosol and Organonitrate Yields from A-Pinene + No3. *J.
750   Phys. Chem. Lett* **2017**, 2826-2834.
751   63.   Teng, A. P.; Crounse, J. D.; Lee, L.; St. Clair, J. M.; Cohen, R. C.; Wennberg, P. O.
752   Hydroxy Nitrate Production in the Oh-Initiated Oxidation of Alkenes. *Atmos. Chem. Phys.* **2015,**
753   *15*, 4297-4316.
754   64.   Griffith, S. M.; Hansen, R. F.; Dusanter, S.; Michoud, V.; Gilman, J. B.; Kuster, W. C.;
755   Veres, P. R.; Graus, M.; de Gouw, J. A.; Roberts, J., et al. Measurements of Hydroxyl and
756   Hydroperoxy Radicals During Calnex-La: Model Comparisons and Radical Budgets. *J. Geophys.
757   Res. - Atmos* **2016,** *121*, 4211-4232.
758   65.   Hidy, G. M.; Blanchard, C. L.; Baumann, K.; Edgerton, E.; Tanenbaum, S.; Shaw, S.;
759   Knipping, E.; Tombach, I.; Jansen, J.; Walters, J. Chemical Climatology of the Southeastern
760   United States, 1999-2013. *Atmos. Chem. Phys.* **2014,** *14*, 11893-11914.
761   66.   Aschmann, S. M.; Reissell, A.; Atkinson, R.; Arey, J. Products of the Gas Phase Reactions
762   of the Oh Radical with A- and B-Pinene in the Presence of No. *J. Geophys. Res. - Atmos* **1998,**
763   *103*, 25553-25561.

764 67.   Jørgensen, S.; Knap, H. C.; Otkjær, R. V.; Jensen, A. M.; Kjeldsen, M. L. H.; Wennberg,
765 P. O.; Kjaergaard, H. G. Rapid Hydrogen Shift Scrambling in Hydroperoxy-Substituted Organic
766 Peroxy Radicals. *J. Phys. Chem. A* **2016,** *120*, 266-275.
767 68.   Massoli, P.; Stark, H.; Canagaratna, M. R.; Krechmer, J. E.; Xu, L.; Ng, N. L.; Mauldin,
768 R. L.; Yan, C.; Kimmel, J.; Misztal, P. K., et al. Ambient Measurements of Highly Oxidized Gas-
769 Phase Molecules During the Southern Oxidant and Aerosol Study (Soas) 2013. *ACS Earth Space*
770 *Chem.* **2018**.
771 69.   Peeters, J.; Nguyen, T. L. Unusually Fast 1,6-H Shifts of Enolic Hydrogens in Peroxy
772 Radicals: Formation of the First-Generation C2 and C3 Carbonyls in the Oxidation of Isoprene. *J.*
773 *Phys. Chem. A* **2012,** *116*, 6134-6141.
774 70.   Praske, E.; Otkjær, R. V.; Crounse, J. D.; Hethcox, J. C.; Stoltz, B. M.; Kjaergaard, H. G.;
775 Wennberg, P. O. Intramolecular Hydrogen Shift Chemistry of Hydroperoxy-Substituted Peroxy
776 Radicals. *J. Phys. Chem. A* **2019,** *123*, 590-600.
777 71.   Paulot, F.; Henze, D. K.; Wennberg, P. O. Impact of the Isoprene Photochemical Cascade
778 on Tropical Ozone. *Atmos. Chem. Phys.* **2012,** *12*, 1307-1325.
779 72.   Wennberg, P. O.; Bates, K. H.; Crounse, J. D.; Dodson, L. G.; McVay, R. C.; Mertens, L.
780 A.; Nguyen, T. B.; Praske, E.; Schwantes, R. H.; Smarte, M. D., et al. Gas-Phase Reactions of
781 Isoprene and Its Major Oxidation Products. *Chem. Rev.* **2018,** *118*, 3337-3390.
782 73.   Arey, J.; Aschmann, S. M.; Kwok, E. S. C.; Atkinson, R. Alkyl Nitrate, Hydroxyalkyl
783 Nitrate, and Hydroxycarbonyl Formation from the Nox−Air Photooxidations of C5−C8 N-Alkanes.
784 *J. Phys. Chem. A* **2001,** *105*, 1020-1027.
785 74.   Matsunaga, A.; Ziemann, P. J. Yields of B-Hydroxynitrates, Dihydroxynitrates, and
786 Trihydroxynitrates Formed from Oh Radical-Initiated Reactions of 2-Methyl-1-Alkenes. *Proc.*
787 *Natl. Acad. Sci. U. S. A* **2010,** *107*, 6664-6669.
788 75.   Cleaves, H. J., Branching Ratio. In *Encyclopedia of Astrobiology*, Gargaud, M.; Amils, R.;
789 Quintanilla, J. C.; Cleaves, H. J.; Irvine, W. M.; Pinti, D. L.; Viso, M., Eds. Springer Berlin
790 Heidelberg: Berlin, Heidelberg, 2011; pp 218-218.
791 76.   Aschmann, S. M.; Atkinson, R.; Arey, J. Products of Reaction of Oh Radicals with A-
792 Pinene. *J. Geophys. Res. - Atmos* **2002,** *107*, ACH 6-1-ACH 6-7.
793 77.   Wisthaler, A.; Jensen, N. R.; Winterhalter, R.; Lindinger, W.; Hjorth, J. Measurements of
794 Acetone and Other Gas Phase Product Yields from the Oh-Initiated Oxidation of Terpenes by
795 Proton-Transfer-Reaction Mass Spectrometry (Ptr-Ms). *Atmospheric Environ.* **2001,** *35*, 6181-
796 6191.
797 78.   Espada, C.; Grossenbacher, J.; Ford, K.; Couch, T.; Shepson, P. B. The Production of
798 Organic Nitrates from Various Anthropogenic Volatile Organic Compounds. *Int. J. Chem. Kinet.*
799 **2005,** *37*, 675-685.
800 79.   Travis, K. R.; Jacob, D. J.; Fisher, J. A.; Kim, P. S.; Marais, E. A.; Zhu, L.; Yu, K.; Miller,
801 C. C.; Yantosca, R. M.; Sulprizio, M. P., et al. Why Do Models Overestimate Surface Ozone in
802 the Southeast United States? *Atmos. Chem. Phys.* **2016,** *16*, 13561-13577.

803

804

805   TOC graphic

806

807

808